

1 **MLL3/4 prevents stem cell hyperplasia and controls differentiation**  
2 **programs in a planarian cancer stem cell model.**

3

4 **Yuliana Mihaylova<sup>1</sup>, Damian Kao<sup>1</sup>, Samantha Hughes<sup>2</sup>, Alvina Lai<sup>1</sup>, Farah**  
5 **Jaber-Hijazi, Nobuyoshi Kosaka<sup>1</sup>, Prasad Abnave<sup>1</sup>, and A. Aziz**  
6 **Aboobaker<sup>1\*</sup>**

7

8 **1. Department of Zoology, Tinbergen Building, South Parks Road,**  
9 **Oxford OX1 3PS, United Kingdom**

10

11 **2. HAN University of Applied Sciences, Institute of Applied Sciences,**  
12 **Laan van Scheut 2, 6525EM, Nijmegen, The Netherlands**

13

14 **Beatson Institute for Cancer Research, Switchback Road, Bearsden,**  
15 **Glasgow G61 1BD**

16

17

18 **\*Author for correspondence**

19 **Aziz.Aboobaker@zoo.ox.ac.uk**

20

## 21 **Background**

22 The family of Mixed Lineage Leukaemia (MLL) histone methyltransferase  
23 proteins are often implicated in disease processes, particularly cancer. Here  
24 we focus on the MLL3 and MLL4 which are mutated in a high percentage of  
25 cancers implicating them as tumour suppressors, but very little is known  
26 about the underlying transcriptional and epigenetic changes that contribute  
27 to cancer.

## 28 **Results**

29 Here we make use of the highly accessible planarians model system to  
30 uncover a role for MLL3/4 in controlling stem cell differentiation and  
31 proliferation, that suggests conservation tumour suppressor over a large  
32 evolutionary timescale function for this epigenetic regulator. Knockdown of  
33 the planarian *Mll3/4* orthologs compromises stem cell differentiation and  
34 leads to hyper-proliferation and tumour-like outgrowth formation. The  
35 planarian system allows as to investigate the epigenetic and transcriptional  
36 studies changes in cells that will go on to form tumours at an early stage  
37 after loss of MLL3/4 function, identifying genome wide changes that occur  
38 early in the development of the pathology. This revealed mis-regulation of  
39 both conserved oncogenes and tumour suppressors, that together likely  
40 explain the cancer-like phenotype observed in planarians.

## 41 **Conclusions**

42 We confirm MLL3/4 tumour suppressor function and uncover a deep  
43 conservation of this role in stem cells. We find potentially conserved mis-  
44 regulated downstream targets driving the effects of MLL3/4 loss of function.  
45 Our work demonstrates the suitability of planarians for the study of  
46 epigenetic phenotypes related to cancer and stem cell function, and for  
47 capturing early causative changes in a definitive population of tumour  
48 forming stem cells *in vivo*.

49

50

51

52

53

54 **Background**

55 The pluripotent adult stem cell (pASC) population of planarian flatworms is a  
56 highly accessible study system to elucidate fundamental aspects of stem cell  
57 function<sup>1,2</sup>. These stem cells, collectively known as neoblasts (NBs), bestow  
58 these animals with an endless capacity to regenerate all the organs and  
59 tissues of this relatively simple organism after amputation. Comparisons of  
60 stem cell expression profiles and available functional data between planarians  
61 and other simpler animals with mammals show that key aspects of stem cell  
62 biology are deeply conserved<sup>3-9</sup>. Thus, studies of the NB population have the  
63 potential to inform us about the origins of fundamental stem cell properties  
64 and behaviors such as maintenance of genome stability<sup>10</sup>, self-renewal<sup>7,11</sup>,  
65 pluripotency<sup>12-15</sup>, differentiation<sup>16-18</sup> and migration<sup>19,20</sup>. All of these are highly  
66 relevant to understanding human disease processes, particularly those  
67 leading to cancer. One exciting prospect is that planarian stem cells may be a  
68 suitable and simple model to study the molecular mechanisms that lead to the  
69 formation of tumor initiating cancer stem cells (CSCs).

70 Many conserved signaling pathways are known to be responsible for  
71 regulating growth, proliferation and other stem cell functions. In disease states  
72 changes in the activity of these pathways can be due to effects on expression  
73 levels, rather than mutations that change proteins, and this can be mediated  
74 epigenetically through chromatin modifications. It is not surprising, therefore,  
75 that mutations in chromatin modifying enzymes, like members of the  
76 Polycomb and Trithorax complexes, are implicated in cancer<sup>21-26</sup>. The  
77 genome-wide effects of chromatin modifying enzymes make understanding  
78 how they contribute to cancer phenotypes very challenging. Complexity in the  
79 form of tissue and cell heterogeneity, life history stage and stage of pathology  
80 make resolution of epigenetic regulatory cause and effect relationships *in vivo*  
81 very challenging. From this perspective, planarians and their accessible and  
82 relatively homogenous stem cell population may be a very useful model  
83 system, especially if the fundamental physiological effects of chromatin

84 modifying complexes are conserved. The system would be particularly  
85 suitable for investigating the early transformative changes in stem cells at the  
86 onset of cancer. Here, we chose to study the planarian ortholog of the human  
87 tumor suppressors Mixed Lineage Leukaemia 3 (MLL3) and MLL4 to further  
88 test the use of planarian NBs as a model of CSCs in the context of epigenetic  
89 histone modifications.

90 The human MLL proteins are the core members of the highly conserved  
91 COMPASS-like (complex of proteins associated with Set1) H3K4 methylase  
92 complexes, and they all contain the 130-140 amino acid SET domain  
93 (Su(var)3-9, Enhancer of zeste and Trithorax). An extensive research effort  
94 has now established the evolutionary history and histone modifying activities  
95 of this extended protein family (**Additional File 1**<sup>27-42</sup>). Perturbation of MLL-  
96 mediated H3K4 methylase activity is characteristic of numerous cancer types.  
97 While the most prominent examples are the translocations widely reported in  
98 leukaemias involving the *Mll1* gene<sup>43-46</sup>, the mutation rate of *Mll3* across  
99 malignancies of different origin approaches 7%, making *Mll3* one of the most  
100 commonly mutated genes in cancer<sup>24</sup>. In attempts to model the role of *Mll3* in  
101 cancer, mice homozygous for a targeted deletion of the *Mll3* SET domain  
102 were found to succumb to urether epithelial tumors at high frequency<sup>32</sup>, an  
103 effect enhanced in a *p53*<sup>+/-</sup> mutational background. Heterozygous deletions  
104 of *Mll3* in mice also lead to acute myeloid leukaemia, implicating *Mll3* in dose-  
105 dependent tumor suppression<sup>26</sup>.

106 Recent studies have revealed an increasingly complicated molecular function  
107 of MLL3, its closely related paralog MLL4, and their partial *Drosophila*  
108 orthologs – LPT (Lost PHD-fingers of trithorax-related; corresponding to the  
109 N-terminus of MLL3/4) and Trr (trithorax-related; corresponding to the C-  
110 terminus of MLL3/4). LPT binds chromatin via its PHD (Plant Homeodomain)  
111 finger domains and targets the H3K4 methylating function of Trr and,  
112 potentially, the H3K27 demethylating action of UTX (Ubiquitously transcribed  
113 tetratricopeptide repeat X), to specific places on the genome<sup>35,39</sup>. LPT-  
114 Trr/MLL3/4 proteins have a role in transcriptional control via monomethylating  
115 and/or trimethylating H3K4 in promoter and enhancer contexts<sup>29,31,33-35,40,47,48</sup>  
116 (**Additional File 1**).

117 Links between cellular hyperplasia, molecular function, and potential  
118 downstream targets of LPT-Trr/MLL3/4 remain to be elucidated. Given the  
119 accessibility of NBs, planarians could provide an informative *in vivo* system for  
120 identifying conserved aspects of MLL3 and MLL4 function relevant to cancer.  
121 We find that the planarian *Mll3/4* homolog, like its *Drosophila* counterpart, has  
122 undergone gene fission leading to split orthologs that are all expressed in  
123 stem cells. Loss of function experiments result in failures in stem cell  
124 differentiation and formation of tumor-like tissue outgrowths caused by stem  
125 cell hyperplasia. These data suggest that fundamental roles in controlling  
126 stem cell behavior might be conserved between planarian and human *Mll3/4*  
127 genes. We performed both RNA-seq and ChIP-seq for key histone  
128 modifications in pre-outgrowth forming NBs to identify downstream effects.  
129 We find that early regulatory changes driving the *Mll3* loss of function cancer-  
130 like phenotype are rooted in mis-regulation of pathways that drive proliferation  
131 and differentiation. Mis-regulated genes include well-established oncogenes  
132 and tumor suppressors and suggest a potentially deep conservation of  
133 MLL3/4-mediated epigenetic regulation in stem cells. We find that  
134 concomitant knockdown of planarian *Mll3/4* and either a *pim-1-like* oncogene  
135 ortholog or a *utx* ortholog, both overexpressed in the *Mll3/4* loss of function  
136 over-proliferation phenotype, can rescue tumor outgrowths. This implicates  
137 these genes as key early regulatory downstream targets important for  
138 controlling stem cell proliferative activity. Our data demonstrate the power of  
139 the planarian model system for actively informing studies in mammalian  
140 systems.

141

## 142 **Results**

143

### 144 **The planarian orthologs of *Mll3/4* are expressed in stem cells**

145 We found 3 partial orthologs of mammalian *Mll3* and *Mll4* genes. The  
146 planarian gene homologous to *Drosophila* LPT and the N-terminus of  
147 mammalian *Mll3/4* was named *Smed-LPT* (KX681482) (**Additional File 2a**).  
148 SMED-LPT (LPT) protein contains two PHD-fingers and a PHD-like zinc-

149 binding domain, suggesting that it has chromatin-binding properties<sup>49</sup> (**Figure**  
150 **1a**). There are two planarian genes homologous to *Drosophila* Trr and the C-  
151 terminus of mammalian *Mll3/4* – *Smed-trr-1* (KC262345) and *Smed-trr-2*  
152 (DN309269, HO004937), both previously described<sup>36</sup>. Both SMED-TRR-1 and  
153 SMED-TRR-2 contain a PHD-like zinc-binding domain, a FYRN (FY-rich N-  
154 terminal domain), FYRC (FY-rich C-terminal domain) and a catalytic SET  
155 domain. SMED-TRR-1 (TRR-1) contains only a single NR (Nuclear Receptor)  
156 box at a non-conserved position and SMED-TRR-2 (TRR-2) has no NR boxes  
157 (**Figure 1a**). This could indicate that the planarian members of the trithorax-  
158 related family are not broadly involved in recognition of nuclear receptors like  
159 their arthropod and mammalian counterparts<sup>33,35,50,51</sup>. It is also possible that  
160 some functional divergence exists between TRR-1 and TRR-2, where only  
161 TRR-1 is capable of interacting with nuclear receptors.

162 We performed wholemount *in situ* hybridization (WISH) and found that *LPT*,  
163 *trr-1* and *trr-2* are broadly expressed across many tissues and organs.  
164 Gamma irradiation, used to remove all cycling cells in *S. mediterranea* within  
165 24 hours, revealed that the three transcripts are also likely to be expressed in  
166 stem cells (**Figure 1b**). This was supported by using an alternative method for  
167 stem cell depletion – *H2B*(RNAi)<sup>7</sup> (**Additional File 2c**). The genes also  
168 showed clear expression in the brain, pharynx and other post-mitotic  
169 differentiated tissues (**Figure 1b**). During regeneration *Mll3/4* gene orthologs  
170 are expressed in structures like the brain and pharynx as those are being  
171 reformed (**Additional File 2b**).

172 In order to confirm expression of all three transcripts in planarian stem cells  
173 we performed double fluorescent *in situ* hybridization (FISH) with the pan-  
174 stem cell marker *Histone2B* (*H2B*). We found conspicuous co-expression  
175 between *LPT*, *trr-1*, *trr-2* and *H2B*, with over 90% of all *H2B*-positive cells co-  
176 expressing the three transcripts (**Figure 1c-d**). These results confirmed the  
177 expression of all three transcripts in cycling cells. Analyses of RNA-seq  
178 experiments consolidated across multiple published Fluorescence Activated  
179 Cell sorting (FACS) datasets<sup>9</sup> revealed that 28% of *LPT*'s total expression is  
180 in the X1 FACS fraction (S/G2/M stem cells), 44% in the X2 fraction (G1 stem  
181 cells and stem cell progeny) and 28% in the X ins fraction (irradiation-

182 insensitive; differentiated cells) of FACS-sorted planarian cell populations  
183 (**Figure 1e**). Both *trr-1* and *trr-2* showed similar distribution in expression  
184 through FACS-sorted cell populations. This is in agreement with the observed  
185 ISH patterns, suggesting all 3 transcripts are widely expressed and co-  
186 expressed in cycling stem cells, stem cell progeny and in neuronal cells  
187 (**Figure 1b-e, Additional File 2d**). These data support the hypothesis that  
188 these proteins act together, with LPT binding chromatin to serve as a scaffold  
189 for TRR methyltransferase activity<sup>35,39</sup>.

190

### 191 **Loss of *Mll3/4* function leads to regeneration defects and tumor-like** 192 **outgrowths**

193 In order to study the function of planarian *Mll3/4*, we investigated phenotypes  
194 after RNAi-mediated knockdown. Following *LPT*(RNAi), there was a clear  
195 failure to regenerate missing structures, including the eyes and pharynx, with  
196 regenerative blastemas smaller than controls (**Figure 2a-b**). After 8 days of  
197 regeneration we observed that, as well as failure to regenerate missing  
198 structures, animals began to form tissue outgrowths (**Figure 2c-d**), with this  
199 phenotype being most pronounced in head pieces (75% of head pieces, 35%  
200 of tail pieces 40% of middle pieces) (**Additional File 3a**). Intact (homeostatic)  
201 *LPT*(RNAi) animals also developed outgrowths, but with decreased frequency  
202 compared to regenerates (**Additional File 3b**).

203 Following individual knockdown of *trr-1* and *trr-2*, milder differentiation defects  
204 were observed compared to *LPT*(RNAi), with no obvious outgrowths  
205 (**Additional File 3, Additional File 4a-f**), confirming results from an earlier  
206 study<sup>36</sup>. However, *trr-1/trr-2* double knockdown recapitulated the phenotype of  
207 *LPT*(RNAi), but with higher penetrance and increased severity (**Additional**  
208 **File 5**). Thus, functional redundancy between the two *trr* paralogs likely  
209 accounts for the reduced severity after individual knockdown. All double  
210 knockdown animals developed outgrowths and started dying as early as day 5  
211 post-amputation. Based on these observations, we decided to focus our  
212 attention on the *LPT*(RNAi) phenotype as regeneration defects and the

213 formation of tissue outgrowths were temporally distinct and could be studied  
214 consecutively.

215 A more thorough study of the differentiation properties of *LPT*(RNAi) animals  
216 following amputation showed that the triclad gut structure failed to regenerate  
217 secondary and tertiary branches and to extend major anterior and posterior  
218 branches (**Figure 2e**). Cephalic ganglia (CG) regenerated as smaller  
219 structures, the two CG lobes did not join in their anterior ends in *LPT*(RNAi)  
220 animals (**Figure 2f**) and the optic chiasma and optic cups were mis-patterned  
221 and markedly reduced (**Figure 2g-h**). We found that 80% of *LPT*(RNAi)  
222 animals did not regenerate any new pharyngeal tissue (**Figure 2i**). We  
223 interpreted these regenerative defects as being indicative of either a broad  
224 failure in stem cell maintenance or in differentiation. The number of NBs  
225 (*H2B*+ve) or early stem cell progeny cells across all lineages (SMEDWI-  
226 1+ve/*H2B*-ve)<sup>52,53</sup> was not affected by perturbation of *LPT* function  
227 (**Additional File 6**). Therefore, we infer that defects in later stem cell progeny  
228 formation and terminal differentiation likely underpin failure in tissue  
229 regeneration. Alternatively, different early stem cell progeny lineages could be  
230 affected in opposite directions depending on their lineage, leading to the  
231 observation of no overall change in the bulk number of early stem cell  
232 progeny (SMEDWI-1+ve/*H2B*-ve).

233

### 234 ***Mll3/4* function is required for correct differentiation of epidermal and** 235 **neural lineages**

236 One of the structures most severely affected following loss of *Mll3/4* function  
237 was the brain. To investigate this further, we looked at the regeneration of  
238 different neuronal subtypes. *LPT*(RNAi) animals had reduced numbers of  
239 GABAergic (**Figure 3a**), dopaminergic (**Figure 3b**), acetylcholinergic (**Figure**  
240 **3c**) and serotonergic (**Figure 3d**) neurons. As expected, the brain defects  
241 were milder following knockdown of *trr-1* or *trr-2* (**Additional File 7a-d**).

242 Among other tissues, the epidermis was also affected. Both early  
243 (*NB.21.11e*+ve cells) and late (*AGAT-1*+ve cells) epidermal progeny cells  
244 were significantly decreased, but not entirely absent, in *LPT*(RNAi)



245 regenerating animals (**Figure 3e**). No such defect was seen in *trr-1* and *trr-2*  
246 knockdown animals (**Additional File 7e**).

247 While we observed defects in the pharynx, neurons, gut and epidermal  
248 progeny, not all lineages were affected by *LPT*(RNAi). Some cell lineages and  
249 organs were correctly regenerated, including protonephridia and ventral and  
250 dorsal cilia (**Additional File 8**).

251 One of the other observable defects in *LPT*(RNAi) animals was abnormal  
252 locomotion, with nearly all worms displaying muscular inch worming rather  
253 than smooth cilia-mediated locomotion. Given differentiation of cilia was  
254 unaffected, it seemed likely this effect was a result of neuronal differentiation  
255 defects, specifically serotonin-dependent control of beating cilia<sup>54</sup>. In  
256 agreement with this interpretation, ectopic serotonin hydrochloride treatment  
257 improved the gliding movement of *Mll3/4* knockdown animals (**Additional File**  
258 **9**).

259 Overall, our data demonstrate that regenerative defects caused by the  
260 abrogation of *Mll3/4* function are associated with broad failures in stem cell  
261 differentiation to produce some but not all lineages.

262

### 263 ***Mll3/4* limits normal stem cell proliferation and tissue growth**

264 Aside from impairment of regeneration following *LPT*(RNAi), the other major  
265 phenotype we observed were outgrowths of tissue that appeared in  
266 unpredictable positions in regenerating pieces. Only two previously reported  
267 planarian RNAi phenotypes have similar pervasive outgrowths of this nature,  
268 and these were caused by hyperplastic stem cell proliferation after knockdown  
269 of other tumor suppressors<sup>55,56</sup>.

270 Planarian regeneration is characterized by an early burst of increased NB  
271 proliferation, 6-12 hours after wounding, and a second peak of proliferation,  
272 48 hours after amputation<sup>53</sup>. Following *LPT*(RNAi), we observed significant  
273 increases in proliferation at both of these peaks and at 8 days post-  
274 amputation, as proliferation fails to return to normal homeostatic levels  
275 (**Figure 4a**). *Trr-1*(RNAi) and *trr-2*(RNAi) animals also show elevated  
276 proliferation in response to amputation (**Additional File 10a**) and similar

277 increases in cell division are seen in knockdown animals that are left  
278 unwounded (**Additional File 10b**).

279 In 8 day-regenerating *LPT*(RNAi) worms the observed over-proliferation is a  
280 result of localized clusters of mitotic cells (**Figure 4b**). Since 8 days of  
281 regeneration is the last stage before outgrowth formation commences, these  
282 clusters likely correspond to sites of future outgrowths (**Figure 4c**). Similar  
283 mitotic clusters are also seen at later stages of regeneration in animals that  
284 are yet to develop outgrowths (**Figure 4d**). We looked specifically in  
285 outgrowths and found mitotic cells (**Figure 4d-e**). NBs not in M-phase (*H2B*-  
286 positive/anti-H3P-negative) are also found outside of their usual  
287 morphological compartments in tissue outgrowths (**Additional File 11**).

288 In order to understand if ectopically cycling NBs represented the breadth of  
289 known stem cell heterogeneity in planarians or only a subset of lineages, we  
290 performed FISH for markers of the *sigma* (collectively pluripotent NBs), *zeta*  
291 (NBs committed to the epidermal lineage) and *gamma* (NBs committed to the  
292 gut lineage) cell populations<sup>57</sup>. We found that different NB populations are  
293 represented in the outgrowths of *LPT*(RNAi) animals. (**Figure 5a, b, c**). Some  
294 outgrowths contain *gamma*+/*Smedwi*- cells (**Figure 5b**), demonstrating that  
295 *LPT*(RNAi) animals form outgrowths comprised of potential cell fates that  
296 would not normally be part of the epidermis.

297 *Sigma*, *zeta* and *gamma* NBs are not significantly increased in pre-outgrowth  
298 *LPT*(RNAi) animals (**Additional File 12**), suggesting that the presence of  
299 these cells in outgrowths is not a secondary effect of increased cell number  
300 and passive spread of these populations.

301 The epidermal progeny markers *NB.21.11e* and *AGAT-1* are concentrated in  
302 the outgrowths of *LPT*(RNAi) animals, while being relatively sparsely  
303 expressed in non-outgrowth tissue (**Additional File 13a**). The observed  
304 disarray of *NB.21.11e*-positive and *AGAT-1*-positive cells in outgrowths could  
305 relate to the perturbed patterning of the epidermal layer in *LPT*(RNAi) animals  
306 (**Additional File 13b**). Epidermal cells appear to have lost polarity and to be  
307 no longer capable of forming a smooth epidermal layer. Furthermore, the  
308 average epidermal nuclear size is significantly increased compared to control

309 **(Additional File 13c)**, an effect similar to the pathology seen following  
310 knockdown of the tumor suppressor *SMG-1*<sup>56</sup>. The epithelial layer in  
311 *LPT*(RNAi) animals also appears less well-defined than that in control  
312 animals, with a blurred distinction between epithelium and mesenchyme.  
313 Another feature of the *LPT*(RNAi) phenotype, encountered in a variety of  
314 malignancies<sup>58</sup>, is changed nuclear shape **(Additional File 13d)**.

315 In summary, LPT controls NB proliferation and restricts stem cells to pre-  
316 defined tissue compartments. Experiments described earlier showed that  
317 LPT, and the other two planarian partial MLL3/4 orthologs, are responsible for  
318 the successful differentiation of some, but not all lineages. Thus, taken  
319 together, our data demonstrate that disturbance of the function of planarian  
320 MLL3/4 COMPASS-like complex by *LPT*(RNAi) leads to development of both  
321 differentiation and proliferation defects with cancer-like features **(Figure 6)**.

322

### 323 ***LPT*(RNAi) results in transcriptional changes consistent with driving** 324 **proliferation in stem cells**

325 A key insight missing from the literature for many tumor suppressors,  
326 including MLL3 and MLL4, is how they regulate the behavior of transformed  
327 stem cells at early stages of cancer. To tackle this question, we decided to  
328 focus on early regeneration when *LPT*(RNAi) animals do not yet exhibit any  
329 outgrowth phenotype. We performed RNA-seq on X1 (G2/M) fluorescence  
330 activated cell sorted (FACS) NBs from *LPT*(RNAi) and *GFP*(RNAi) planarians  
331 at 3 days of regeneration. Our analysis revealed that 540 transcripts are  
332 down-regulated (fold change  $\leq -1.5$ ,  $p < 0.05$ ) and 542 up-regulated (fold  
333 change  $\geq 1.5$ ,  $p < 0.05$ ) in X1 stem cells from *LPT*(RNAi) animals when  
334 compared to controls **(Additional file 20)**.

335 A recent meta-analysis of all available *S. mediterranea* RNA-seq data allowed  
336 classification of all expressed loci in the planarian genome by their relative  
337 expression in FACS sorted cell populations representing stem cells, stem cell  
338 progeny and differentiated cells<sup>9</sup>. Superimposing the differentially expressed  
339 genes following *LPT*(RNAi) onto a gene expression spectrum reflecting FACS  
340 compartments shows that *LPT*(RNAi) has a broad effect on gene expression

341 in X1 cells (**Figure 7a**), affecting genes normally expressed in many different  
342 planarian cell compartments (**Figure 7b**). These findings confirm that  
343 *LPT*(RNAi) has a complex effect, influencing different gene classes, including  
344 47 transcription factors, in stem cells.

345 Analysis of Gene Ontology (GO) terms revealed a clear enrichment for cell  
346 cycle and cell division-associated terms in the list of up-regulated genes  
347 (**Figure 7c**), in agreement with the observed hyperproliferation in *LPT*(RNAi)  
348 phenotype. The list of down-regulated genes is also enriched for cell cycle-  
349 related terms, as well as cell differentiation and metabolism-related processes  
350 (**Figure 7c**). Genes associated with metabolic processes have been  
351 previously shown to be down-regulated following *Mll3/4* loss of function<sup>50,59</sup>.

352

### 353 ***LPT*(RNAi)-induced changes to promoter H3K4 methylation and** 354 **transcription are correlated**

355 Previous studies tie MLL3/4/*LPT*-Trr function directly to mono- and tri-  
356 methylation of H3K4<sup>29,31-34</sup> and indirectly to trimethylation of H3K27, because  
357 the H3K27me3 demethylase UTX is present in the same protein complex<sup>60</sup>.  
358 In order to understand potential epigenetic causes of the transcriptional  
359 changes following *LPT*(RNAi), we also performed ChIP-seq on X1 cells. The  
360 profile of H3K4me3, H3K4me1 and H3K27me3 in control X1 cells showed that  
361 genes enriched in X1 stem cells have the highest H3K4me3 and the lowest  
362 H3K27me3 signal at predicted transcriptional start sites (TSSs), consistent  
363 with active transcription of these genes (**Figure 8a, Additional File 14**). We  
364 observed the reverse pattern for genes enriched in differentiated cells,  
365 consistent with repressed transcription. Furthermore, the peak in H3K4me1  
366 signal is shifted downstream and away from the TSS for genes with enriched  
367 expression in X1 NBs, allowing for active transcription. Conversely, the peak  
368 in H3K4me1 is positioned across the TSS for genes with enriched expression  
369 in differentiated cells and no or relatively low expression in NBs, indicative of  
370 repressed transcription in NBs. These data are in agreement with previous  
371 reports in planarians and mammalian cells<sup>9,34,37</sup>.

372 *LPT*(RNAi) led to a broad decrease in the level of both H3K4me3 and  
373 H3K4me1 from just upstream and across the TSSs throughout the genome,  
374 consistent with an active role for MLL3/4 in deposition of these histone  
375 modifications. This was particularly true for the H3K4me1 mark at the TSSs of  
376 genes whose expression is normally enriched in differentiated cells (**Figure**  
377 **8a, Additional File 15a**). Concomitant with this, we also observed an  
378 increase in H3K4me1 signal upstream of the predicted TSS (**Figure 8a,**  
379 **Additional File 15a**). For the H3K27me3 mark, no clear pattern was  
380 observed across the genome as result of *LPT*(RNAi) in any group of genes  
381 subdivided by FACS compartment expression profiles.

382 We next looked more closely at the promoter histone methylation status of  
383 those genes whose transcript levels were affected by *LPT*(RNAi) (**Additional**  
384 **File 15b**). Most notably, for genes enriched for X1 NB expression, we  
385 observed an inverse relationship between expression following *LPT*(RNAi)  
386 and amount of TSS-proximal H3K4me1. This suggests that *LPT*(RNAi) leads  
387 to a reduction of this repressive mark at these loci and subsequent up-  
388 regulation of expression in stem cells. For mis-regulated genes not enriched  
389 in X1 NBs, we observed instead a positive correlation between changes in  
390 transcriptional expression and changes in H3K4me3 levels (**Figure 8b**).  
391 Overall, our data suggest that reductions in H3K4me1 following *LPT*(RNAi)  
392 cause up-regulation of some of the stem cell genes implicated by our RNA-  
393 seq data from *LPT*(RNAi) animals, while reductions in H3K4me3 are related  
394 to down-regulation of non-NB enriched genes.

395 Our data demonstrate that key features of promoter-centric histone  
396 modification-mediated control of transcription are conserved between  
397 planarians and mammals, as previously shown<sup>9,37</sup>. Consistent with MLL3/4's  
398 known role in H3K4 methylation, changes in gene expression following  
399 *LPT*(RNAi) are correlated with the amount of H3K4me1 and H3K4me3.

400

401 ***LPT*(RNAi) leads to up-regulation of known and putative oncogenes and**  
402 **down-regulation of tumor suppressors**

403 After observing the global changes in expression and histone modification  
404 patterns following *LPT*(RNAi), we wanted to identify individual mis-regulated  
405 genes that could potentially be major contributors to the differentiation and  
406 tumor-like phenotype, and assess which of these were potentially direct or  
407 indirect targets of MLL3/4 activity in stem cells.

408 The well-known tumor suppressor *p53*, where hypomorphic loss of function  
409 has been previously shown to cause dorsal outgrowths in planarians<sup>61</sup>, was  
410 found to be significantly down-regulated in X1 stem cells after *LPT*(RNAi)  
411 (**Figure 9a**). Consistent with this, we observed a small decrease in H3K4me3  
412 around the promoter region. Other cancer-related genes, like the tumor  
413 suppressor *PR domain zinc finger protein 1* (*PRDM1*, also known as *Blimp-1*)  
414 and the Polycomb gene *Suppressor of zeste 12* (*Su(z)12*) also had  
415 significantly altered expression following *LPT*(RNAi), both correlating with  
416 changes in H3K4me3 levels. While an increase in H3K4me3 on the *Su(z)12*  
417 promoter would not be predicted as an effect caused by *LPT*(RNAi), elevated  
418 levels of the H3K4me3 are consistent with up-regulation and may result from  
419 subtle effects on H3K4me1 levels.

420 The *pituitary homeobox* (*pitx*) gene was also significantly up-regulated in  
421 expression and had elevated levels of H3K4me3 on its promoter. *Pitx* is  
422 expressed in the serotonergic neuronal precursor cells<sup>54,62</sup> and thus, in  
423 planarians, it is not directly implicated in stem cell proliferation, but rather in  
424 differentiation. Nonetheless, the fact that *LPT*(RNAi) led to *pitx* up-regulation  
425 was of great interest for two reasons. Firstly, we knew that serotonergic  
426 neurons require PITX function or fail to regenerate in planarians<sup>54,62</sup> and,  
427 secondly, in human medulloblastomas down-regulation of *Mll3* and over-  
428 expression of *pitx2* are co-occurrences (Pomeroy Brain Oncomine dataset<sup>63</sup>  
429 ([www.oncomine.org](http://www.oncomine.org))) (**Figure 9b**). To investigate the cellular basis for *pitx*  
430 overexpression, we performed FISH for this gene in *LPT*(RNAi) animals. We  
431 observed an accumulation of *pitx*-positive cells in *LPT*(RNAi) regenerates  
432 (**Figure 9c**). Given that production of terminally differentiated serotonergic  
433 neurons is decreased (**Figure 3d**), the increase of *pitx*-positive cells following  
434 *LPT*(RNAi) marks the accumulation of serotonergic neuronal precursors that  
435 fail to differentiate. Whether *pitx* up-regulation is causal or just a marker in the

436 failure of serotonergic neuron regeneration is not clear, but MLL3/4/LPT-Trr  
437 activity does control the maturation of serotonergic neuronal precursors into  
438 serotonergic neurons. The *LPT*(RNAi)-dependent up-regulation of *pitx* might  
439 also be a conserved feature of MLL3/4 mis-regulation in some cancer types  
440 <sup>63</sup>.

441 While we observed an agreement between expression levels and changes in  
442 H3K4me3 around the TSS for many mis-regulated genes, this was not the  
443 case for all genes. One example where transcriptional expression is  
444 significantly up-regulated, but H3K4me3 levels are slightly down-regulated is  
445 *utx* (**Figure 10a**). This finding suggests that for some mis-regulated genes  
446 there is no direct relationship between LPT activity at their promoter regions  
447 and gene expression. The effect on *utx* expression is particularly significant as  
448 UTX itself may interact with MLL3/4/LPT-Trr and regulate gene expression  
449 across the genome.

450 We identified two planarian orthologs of the serine/threonine kinase oncogene  
451 *pim-1* (*Smed-pim-1* and *Smed-pim-1-like* or *pim-1* and *pim-1-like* in short) with  
452 increased levels of expression in stem cells following *LPT*(RNAi). Like *utx*,  
453 *pim-1* (KY849969) did not show an increase in H3K4me3 levels on its  
454 promoter. For *pim-1-like* (KY849970), whose expression is enriched in NBs,  
455 promoter-proximal H3K4me1 levels were examined instead, based on  
456 previous correlation analysis (**Figure 8b**) establishing H3K4me1 as the most  
457 predictive mark of transcriptional expression for X1 enriched genes. We  
458 observed that H3K4me1 was decreased at the *pim-1-like* TSS, consistent with  
459 increased transcriptional levels. These data suggest *pim-1-like* is a direct  
460 MLL3/4 target. Observation of these two orthologs of the *pim* kinase  
461 oncogene and *utx* suggests that up-regulated genes identified in the RNA-seq  
462 dataset include those with and without correlated changes in histone  
463 modification patterns at promoters. Other genes associated with cancer and  
464 development were also mis-regulated following *LPT*(RNAi) with patterns of  
465 H3K4 methylation that were both consistent and inconsistent with changes in  
466 transcript levels (**Additional File 16**).

467 The up-regulation of *pim-1* has been associated with genome instability <sup>64</sup> and  
468 onset of malignancy <sup>65,66</sup>, while the up-regulation of the MLL3/4 partner and

469 H3K27me3 demethylase, *utx*, has been implicated in increased proliferation  
470 and tumor invasiveness<sup>67</sup>. Based on this, the overexpression of *utx*, *pim-1*  
471 and *pim-1-like* together represented some of the best candidates for major  
472 effects amongst those with significant up-regulation in expression. In order to  
473 test whether the up-regulated expression of *pim-1*, *pim-1-like* or *utx* is  
474 potentially key to the *LPT*(RNAi) cancer-like phenotype, we attempted  
475 *LPT*(RNAi) rescue experiments in the form of double RNAi knockdowns  
476 (**Additional File 17**). At 48 hours post-amputation, *LPT*(RNAi) regenerates  
477 have a significantly increased stem cell proliferation (**Figure 4a, b**) and so do  
478 *GFP/LPT*(RNAi) double knockdown animals (**Figure 10b**). Whereas *LPT/pim-1*(RNAi)  
479 regenerates still have elevated NB proliferation, both *LPT/pim-1-like*(RNAi)  
480 and *LPT/utx*(RNAi) regenerates have a significantly decreased NB  
481 proliferation compared to *GFP/LPT*(RNAi), and half as many animals in these  
482 two conditions went on to form outgrowths (**Figure 10c**). These findings  
483 suggest that the up-regulation of both *pim-1-like* and *utx* are involved in  
484 driving the *LPT*(RNAi) animals' cancer-like phenotype. *Pim-1-like*'s up-  
485 regulation in *LPT*(RNAi) planarians may be directly connected to changing  
486 histone modifications at its promoter, while *utx*'s up-regulation is likely not due  
487 to a direct effect on a promoter region (**Figure 10a**).

488 Our study not only shows a conserved physiological role in controlling cell  
489 proliferation for the conserved MLL3/4 gene family, but also has allowed us to  
490 identify novel gene targets of LPT and MLL3/4-mediated transcriptional  
491 control in stem cells and begin to elucidate the mechanisms behind *Mll3/4*  
492 loss of function phenotypes. Some of these mechanisms are also likely to be  
493 conserved in mammals.

494

## 495 **Discussion**

496 *Mll3* and *Mll4* have been implicated<sup>24</sup> in different malignancy landscapes<sup>24</sup>, with  
497 clear evidence for tumor suppressor roles in mammalian systems<sup>26,32,68</sup>. Our  
498 study demonstrates that loss of function of the planarian *Mll3/4* ortholog also  
499 results in the emergence of a cancer-like phenotype characterized by  
500 differentiation and proliferation defects. Our work shows that LPT, TRR-1 and



501 TRR-2 control differentiation to form many (gut, eyes, brain, pharynx), but not  
502 all lineages (cilia, protonephridia), suggesting that the MLL3/4 COMPASS-like  
503 complex is not a universal and unilateral regulator of differentiation. This  
504 conclusion is supported by the opposing effects of *LPT*(RNAi) on different  
505 lineages of stem cell progeny production. For example, while epidermal NB  
506 progeny (*NB.21.11e*- and *AGAT-1*-positive cells) were decreased, the number  
507 of serotonergic neuronal precursors (*pitx*-positive cells) was increased. Such  
508 differential effects might be related to the diverse molecular function of  
509 MLL3/4 proteins, associated with both positive and negative regulation of  
510 transcription via control of both enhancer and promoter activity<sup>29,31,33-35</sup>.  
511 Future work in planarians will allow closer investigation of these and other  
512 epigenetic effects on stem cell function. Study of enhancers, in particular, will  
513 benefit from further improvements in planarian genome assemblies, to allow  
514 both epigenetic and comparative genomic methods for enhancer detection.

515 We found that clusters of mitotic cells preceded the appearance of outgrowths  
516 in *LPT*(RNAi) regenerating animals, likely pre-empting where the outgrowths  
517 would subsequently form. The observation of clusters of cells and the  
518 formation of outgrowths in some but not all RNAi animals suggests a  
519 heterogeneity in stem cell responses to *LPT*(RNAi). This probably reflects the  
520 stochastic nature of the broad genome wide epigenetic changes that will have  
521 some variability between cells, such that only some cells cycle out of control  
522 and cause outgrowths. We also observed that outgrowth tissue contained  
523 different classes of stem cells. Among these stem cells, the presence of  
524 sigma NBs (thought to include truly pluripotent stem cells<sup>57</sup> is of particular  
525 significance. When mis-regulated, these cells could share fundamental  
526 similarities with cancer stem cells (CSCs) often found in human malignancies  
527<sup>69</sup>. CSCs have been described as one of the main factors in cancer  
528 aggressiveness and resistance to treatment<sup>70</sup>. Studying such cells in a simple  
529 *in vivo* stem cell model provided by the planarian system should bring further  
530 insight into important control mechanisms that are mis-regulated in different  
531 cancers. Our work here provides a useful example of this approach.

532 Our data suggest that *LPT* regulates expression of genes across cell types,  
533 including some genes with enriched expression in stem cells. Genes with

534 significant expression differences following *LPT* knockdown were mostly  
535 associated with cell proliferation, differentiation and metabolic processes. A  
536 subset of genes where RNA-seq and ChIP-seq data correlate are likely a  
537 direct consequence of *LPT*(RNAi) affecting promoter histone methylation  
538 status. Genes with altered expression where there is no such correlation, may  
539 represent indirect (secondary) changes or, alternatively, may have enhancers  
540 that have altered histone modifications as a result of *LPT*(RNAi). Future work  
541 will develop the use of planarians as a model of epigenetic gene regulation  
542 and allow further investigation.

543 One of the most famous and well-studied tumor suppressors – *p53*, was  
544 significantly down-regulated following *LPT*(RNAi). *P53* acts as a cell cycle  
545 checkpoint guardian and has been reported to undergo mutations in more  
546 than 40% of all cancers<sup>24</sup>. *P53*(RNAi) planarians exhibit hyper-proliferation  
547 and outgrowth formation (dependent on the dose), suggesting some  
548 conservation of function<sup>61</sup>. Studies in mice have postulated that *Mll3*'s role in  
549 cancer is (at least partially) dependent on *p53* function<sup>26,32</sup> and this may also  
550 be the case in planarians.

551 Many of the genes overexpressed as a result of *LPT*(RNAi) may have roles in  
552 driving inappropriate stem cell activity, and some of these may be directly  
553 regulated by MLL3/4. For example, the expression of the H3K27me3  
554 demethylase, *utx*, was significantly increased in stem cells following  
555 *LPT*(RNAi). UTX is itself a part of the MLL3/4/Trithorax-related protein  
556 complex<sup>60,71</sup> and UTX protein and mRNA overexpression has been linked to  
557 increased cell proliferation and invasiveness in breast cancer<sup>67</sup>. Our RNA-seq  
558 results also identified two planarian homologs of the oncogene *pim-1*, called  
559 *Smed-pim-1* and *Smed-pim-1-like*, that were overexpressed in stem cells  
560 following *LPT*(RNAi). Amongst overexpressed genes, these represented likely  
561 candidates for contributing to the *LPT*(RNAi). Overexpressed target genes  
562 can potentially be validated as having a role in *Mll3/4* loss of function  
563 pathology in planarians by double RNAi experiments. We found that double  
564 RNAi with either *utx* or *pim-1-like*, was sufficient to rescue *Mll3/4* loss of  
565 function over-proliferation and outgrowth phenotypes induced by *LPT*(RNAi).  
566 This provides strong support for the hypothesis that the over-expression of

567 these two genes was significant in driving stem cell hyperplasia. These  
568 experiments demonstrate the value of our approach to identify potential  
569 downstream targets and implicate novel regulatory interactions driving the  
570 *Mll3/4* loss of function phenotype. These targets can now be tested for  
571 conservation in mammalian experimental systems.

572

## 573 **Conclusion**

574 In conclusion, our study confirms conservation of function between  
575 mammalian *Mll3* and *Mll4* genes and their planarian orthologs. We identified  
576 candidates that are mis-regulated by *LPT*(RNAi) that may be conserved  
577 targets of MLL3/4 and may help explain how *Mll3/4* loss of function mutations  
578 contribute to human cancers. These findings demonstrate the strength of the  
579 planarian system for understanding fundamental stem cell mechanisms and  
580 its potential for in-depth investigation of epigenetic mis-regulation in cancer-  
581 causing stem cells.

582

## 583 **Methods**

### 584 *Animal husbandry*

585 Asexual freshwater planarians of the species *S. mediterranea* were used. The  
586 culture was maintained in 1x Montjuic salts water<sup>72</sup>. Planarians were fed  
587 organic calf liver once a week. After every feeding, the water was changed.  
588 Planarians were starved for 7 days prior to each experiment. They were also  
589 starved throughout the duration of each experiment.

590

### 591 *RNAi*

592 Double-stranded RNA (dsRNA) was synthesized from DNA fragments cloned  
593 in pCRII (Invitrogen) or pGEM-T Easy (Promega) vectors. T7 (Roche) and  
594 SP6 (NEB) RNA polymerases were used for transcription of each strand. The  
595 two transcription reactions were combined upon ethanol precipitation. RNA  
596 was denatured at 68 °C and re-annealed at 37 °C. Quantification was  
597 performed on a 1% agarose gel and Nanodrop spectrophotometer.

598 For single RNAi experiments a working concentration of 2 µg/µl was used. For  
599 double RNAi, each gene's RNA was at a concentration 4 µg/µl, resulting in  
600 solution concentration of 2 µg/µl.

601 DsRNA was delivered via microinjection using Nanoject II apparatus  
602 (Drummond Scientific) with 3.5" Drummond Scientific (Harvard Apparatus)  
603 glass capillaries pulled into fine needles on a Flaming/Brown Micropipette  
604 Puller (Patterson Scientific). Each animal received around 100 nl dsRNA each  
605 day. *H2B*(RNAi) was performed for three consecutive days, as per Solana et  
606 al.'s (2012) protocol. For single and double *LPT*, *trr-1* and *trr-2* knockdown, a  
607 course of 7 days of microinjections was performed (3 consecutive days + 2  
608 days rest + 4 consecutive days). *Set1*(RNAi) and *utx*(RNAi) were performed  
609 for 4 consecutive days.

610 Primers used for amplification of DNA for dsRNA synthesis can be found in  
611 **Supplementary Table 2**.

612

### 613 *In situ hybridization*

614 RNA probes labeled with digoxigenin and fluorescein were generated via anti-  
615 sense transcription of DNA cloned in PCRII (Invitrogen) or PGemTEasy  
616 (Promega) vector. *In situ* hybridization was performed as described in King  
617 and Newmark's (2013) protocol for most fluorescent experiments. For *LPT*,  
618 *trr-1*, *trr-2*, *sigma*, *zeta* and *gamma* fluorescent *in situ* procedures, a pooled  
619 probes method was used, as described in van Wolfswinkel et al.<sup>57</sup>.  
620 Colorimetric *in situ* hybridization procedures were performed as described in  
621 Gonzalez-Estevez et al.<sup>73</sup>. Primers used for amplification of DNA for RNA  
622 probe synthesis can be found in (**Additional File 21**).

623

### 624 *Immunohistochemistry*

625 Immunohistochemistry was performed as described in Cebria and Newmark<sup>74</sup>.  
626 Antibodies used were: anti-H3P (phosphorylated serine 10 on histone H3;  
627 Millipore; 09-797; 1:1000 dilution), anti-VC1 (kindly provided by Prof. Hidefumi  
628 Orii (check title); 1:10000 dilution), anti-SMEDWI-1 (kindly provided by Prof.

629 Jochen Rink; 1:500 dilution), anti-SYNORF-1 (3C11; Developmental Studies  
630 Hybridoma Bank; 1:50 dilution), anti-acetylated tubulin (Developmental  
631 Studies Hybridoma Bank; 1:200 dilution).

632

### 633 *Imaging and image analysis*

634 Colorimetric images were taken on Zeiss Discovery V8 (Carl Zeiss)  
635 microscope with a Canon EOS 600D or Canon EOS 1200D camera.  
636 Fluorescent images were taken on either Inverted Olympus FV1000 or  
637 FV1200 Confocal microscope. Cells were counted via Adobe Photoshop CS6  
638 or FIJI software and the count was normalized to imaged area in mm<sup>2</sup>.

639

### 640 *Flow cytometry*

641 A modified version of Romero et al.'s<sup>75</sup> planarian FACS protocol was used, as  
642 described in Kao et al.<sup>9</sup>. A FACS Aria III machine equipped with a violet laser  
643 was used for the sort. BD FACSDiva and FlowJo software was used for  
644 analysis and gate-setting.

645

### 646 *Western blot*

647 2xLaemmli buffer (Sigma Aldrich), 1M DTT and cOmplete protease inhibitors  
648 (Roche) were used for protein extraction from 10-15 animals per condition.  
649 Protein extract was quantified with Qubit Protein Assay kit (Thermo Fisher  
650 Scientific). NuPAGE Novex 4-12% Bis-Tris protein gels (Thermo Fisher  
651 Scientific) were used, followed by a wet transfer in a Mini Trans-Blot  
652 Electrophoretic Transfer Cell machine. Ponceau S (Sigma Aldrich) whole-  
653 protein stain was used prior to antibody incubation. The antibodies used were:  
654 anti-H3 (unmodified histone H3; rabbit polyclonal; Abcam; ab1791; 1:10000  
655 dilution), anti-H3K4me3 (rabbit polyclonal; Abcam; ab8580; 1:1000 dilution),  
656 anti-H3K4me1 (rabbit polyclonal; Abcam; ab8895; 1:1000 dilution), anti-  
657 H3K27me3 (mouse monoclonal; Abcam; ab6002; 1:1000 dilution), anti-mouse  
658 IgG HRP-linked antibody (Cell Signalling; 7076P2), anti-rabbit IgG HRP-linked

659 antibody (Cell Signalling; 7074P2). The experiments were done to validate the  
660 specificity of the histone modification antibodies (**Additional File 18**).

661

#### 662 *ChIP-seq*

663 600000-700000 planarian x1 cells were FACS-sorted (using 3-day knockdown  
664 regenerates) in PBS and pelleted at 4 °C. During the pelleting, S2 cells were  
665 added (corresponding to roughly 15% of the number of planarian x1 cells) for  
666 the purpose of downstream data normalisation. Samples were then processed  
667 as described in Kao et al. (2017). The process is summarized in **Additional**  
668 **File 19**. The libraries were sequenced on an Illumina NextSeq machine.  
669 Three biological replicates were prepared. The raw reads are available in the  
670 Short Read Archive (PRJNA338116).

671

#### 672 *RNA-seq*

673 300000 x1 NBs were FACS-sorted in RNALater (Ambion) from knockdown  
674 animals at 3 days of regeneration. Cells were pelleted at 4 °C and Trizol-  
675 based total RNA extraction was performed. The amount of total RNA used for  
676 each library preparation was 0.8-1 µg. Illumina TruSeq Stranded mRNA LT kit  
677 was used for library preparation. The kit instructions were followed. Libraries  
678 were quantified with Qubit, Agilent Bioanalyzer and KAPA Library  
679 Quantification qPCR kit. Samples were sequenced on an Illumina NextSeq  
680 machine. Two biological replicates were prepared. The raw reads are  
681 available in the Short Read Archive (PRJNA338115).

682

#### 683 *ChIP-seq data analysis*

684 ChIP-seq reads were trimmed with Trimmomatic 0.32<sup>76</sup> and aligned to the *S.*  
685 *mediterranea* SmedGD asexual genome 1.1<sup>77</sup> and *D.melanogaster* genome  
686 r6.10<sup>78</sup> with BWA mem 0.7.12. Picard tools 1.115 was used to remove read  
687 duplicates after mapping. Python scripts were used to filter and separate out  
688 read pairs belonging to either genome. ChIP-seq coverage tracks were then

689 generated and normalized according to Orlando et al.<sup>79</sup>. For more in-depth  
690 methods, including code, refer to the **Supplementary Python Notebook**.

691

#### 692 *RNA-seq data analysis*

693 Raw reads were trimmed with Trimmomatic 0.32<sup>76</sup> and pseudo-aligned to a  
694 set of asexual genome annotations described in Kao et al. (2017) with Kallisto  
695 0.42<sup>80</sup>. Differential expression was subsequently performed with Sleuth  
696 0.28.1<sup>81</sup>. For more in-depth methods, including code, refer to the  
697 **Supplementary Python Notebook**.

698

#### 699 *Statistical methods*

700 Wherever cell number was compared between experimental condition and  
701 control, a 2-tailed ttest assuming unequal variance was used. Each legend  
702 states the number of specimens per condition, where relevant. Bar graphs  
703 show the mean average and the error bars are always Standard Error of the  
704 Mean.

705 For analysis of RNA-seq data, Wald's test (as part of the Sleuth<sup>82</sup> software)  
706 was used for assessing differential expression. Spearman's rank correlation  
707 was used for assessing the correlation between RNA-seq and ChIP-seq data.  
708 Hypergeometric tests were used for assessing enrichment in the RNA-seq  
709 data.

710

#### 711 *Data availability*

712 The ChIP-seq and RNA-seq datasets are deposited in the Short Read Archive  
713 with accession numbers: PRJNA338116 and PRJNA338115 respectively).  
714 The 'Pomeroy Brain' dataset<sup>63</sup> from the oncomine database  
715 (<https://www.oncomine.com>) was used for assessing expression level of *pitx2*  
716 and *Mll3* in human medulloblastoma versus normal cerebellum. All other data  
717 availability is either within the article (and its supplementary information) or  
718 available upon request.

719

## 720 **Declarations**

### 721 *Competing interests*

722 The authors declare they have no competing interests.

### 723 *Funding*

724 This work was funded by grants from the Medical Research Council (grant  
725 number MR/M000133/1) and the Biotechnology and Biological Sciences  
726 Research Council (grant number BB/K007564/1) to AA. A.G.L. is funded by a  
727 Human Frontier Science Program fellowship.

### 728 *Authors' contributions*

729 AA and YM conceived and designed the study. YM performed the  
730 experiments. DK performed the bioinformatic analyses. SH participated in the  
731 optimization of the ChIP-seq protocol. AGL participated in the optimization of  
732 the RNA-seq protocol. FJH performed initial work on the project, including  
733 generating the first *LPT*(RNAi) results. NK and PA helped with sigma, zeta  
734 and gamma *in situ* hybridization experiments. YM and AA wrote the  
735 manuscript.

### 736 *Acknowledgements*

737 We thank past and present members of the AA lab for comments on the  
738 manuscript.

739

740

## 741 **References**

- 742 1. Aboobaker, A. A. Planarian stem cells: a simple paradigm for  
743 regeneration. *Trends in Cell Biology* **21**, 304–311 (2011).
- 744 2. Rink, J. C. Stem cell systems and regeneration in planaria. *Dev Genes*  
745 *Evol* **223**, 67–84 (2012).
- 746 3. Onal, P. *et al.* Gene expression of pluripotency determinants is  
747 conserved between mammalian and planarian stem cells. *The EMBO*  
748 *Journal* **31**, 2755–2769 (2012).
- 749 4. Adamidi, C. *et al.* De novo assembly and validation of planaria  
750 transcriptome by massive parallel sequencing and shotgun proteomics.  
751 *Genome Research* **21**, 1193–1200 (2011).



- 752 5. Labbé, R. M. *et al.* A Comparative Transcriptomic Analysis Reveals  
753 Conserved Features of Stem Cell Pluripotency in Planarians and  
754 Mammals. *STEM CELLS* **30**, 1734–1745 (2012).
- 755 6. Solana, J. *et al.* Conserved functional antagonism of CELF and MBNL  
756 proteins controls stem cell-specific alternative splicing in planarians.  
757 *eLife* **5**, 1193 (2016).
- 758 7. Solana, J. *et al.* Defining the molecular profile of planarian pluripotent  
759 stem cells using a combinatorial RNA-seq, RNA interference and  
760 irradiation approach. *Genome Biol.* **13**, R19 (2012).
- 761 8. Alié, A. *et al.* The ancestral gene repertoire of animal stem cells. *Proc*  
762 *Natl Acad Sci USA* **201514789–8** (2015).  
763 doi:10.1073/pnas.1514789112
- 764 9. Kao, D., Mihaylova, Y., Hughes, S., Lai, A. & Aboobaker, A. Epigenetic  
765 analyses of the planarian genome reveals conservation of bivalent  
766 promoters in animal stem cells. *bioRxiv* 122135 (2017).  
767 doi:10.1101/122135
- 768 10. Shibata, N. *et al.* Inheritance of a Nuclear PIWI from Pluripotent Stem  
769 Cells by Somatic Descendants Ensures Differentiation by Silencing  
770 Transposons in Planarian. *Developmental Cell* **37**, 226–237 (2016).
- 771 11. Salvetti, A. DjPum, a homologue of Drosophila Pumilio, is essential to  
772 planarian stem cell maintenance. *Development* **132**, 1863–1874 (2005).
- 773 12. Reddien, P. W. Specialized progenitors and regeneration. *Development*  
774 **140**, 951–957 (2013).
- 775 13. Juliano, C. E., Swartz, S. Z. & Wessel, G. M. A conserved germline  
776 multipotency program. *Development* **137**, 4113–4126 (2010).
- 777 14. Jaber-Hijazi, F. *et al.* Planarian MBD2/3 is required for adult stem cell  
778 pluripotency independently of DNA methylation. *Developmental Biology*  
779 **384**, 141–153 (2013).
- 780 15. Scimone, M. L., Meisel, J. & Reddien, P. W. The Mi-2-like Smed-CHD4  
781 gene is required for stem cell differentiation in the planarian *Schmidtea*  
782 *mediterranea*. *Development* **137**, 1231–1241 (2010).
- 783 16. Zhu, S. J., Hallows, S. E., Currie, K. W., Xu, C. & Pearson, B. J. A mex3  
784 homolog is required for differentiation during planarian stem cell lineage  
785 development. *eLife* **4**, 304 (2015).
- 786 17. Cowles, M. W., Omuro, K. C., Stanley, B. N., Quintanilla, C. G. & Zayas,  
787 R. M. COE Loss-of-Function Analysis Reveals a Genetic Program  
788 Underlying Maintenance and Regeneration of the Nervous System in  
789 Planarians. *PLoS Genet* **10**, e1004746–12 (2014).
- 790 18. Barberan, S., Fraguas, S. & Cebrià, F. The EGFR signaling pathway  
791 controls gut progenitor differentiation during planarian regeneration and  
792 homeostasis. *Development* **143**, 2089–2102 (2016).
- 793 19. Guedelhofer, O. C. & Alvarado, A. S. Amputation induces stem cell  
794 mobilization to sites of injury during planarian regeneration.  
795 *Development* **139**, 3510–3520 (2012).
- 796 20. Abnave, P. *et al.* A shielded irradiation assay to investigate mechanisms  
797 of in vivo stem cell migration in planarians. 1–42 (2016).  
798 doi:10.1101/080853
- 799 21. Varambally, S. *et al.* The polycomb group protein EZH2 is involved in  
800 progression of prostate cancer. *Nature* **419**, 624–629 (2002).
- 801 22. Villa, R. *et al.* Role of the Polycomb Repressive Complex 2 in Acute

- 802 Promyelocytic Leukemia. *Cancer Cell* **11**, 513–525 (2007).
- 803 23. Parsons, D. W. *et al.* The genetic landscape of the childhood cancer  
804 medulloblastoma. *Science* **331**, 435–439 (2011).
- 805 24. Kandoth, C. *et al.* Mutational landscape and significance across 12  
806 major cancer types. *Nature* **502**, 333–339 (2013).
- 807 25. Gui, Y. *et al.* Frequent mutations of chromatin remodeling genes in  
808 transitional cell carcinoma of the bladder. *Nature Publishing Group* **43**,  
809 875–878 (2011).
- 810 26. Chen, C. *et al.* MLL3 Is a Haploinsufficient 7q Tumor Suppressor in  
811 Acute Myeloid Leukemia. *Cancer Cell* **25**, 652–665 (2014).
- 812 27. Shilatifard, A. The COMPASS Family of Histone H3K4 Methylases:  
813 Mechanisms of Regulation in Development and Disease Pathogenesis.  
814 *Annu. Rev. Biochem.* **81**, 65–95 (2012).
- 815 28. Wu, M. *et al.* Molecular Regulation of H3K4 Trimethylation by Wdr82, a  
816 Component of Human Set1/COMPASS. *Molecular and Cellular Biology*  
817 **28**, 7337–7344 (2008).
- 818 29. Herz, H. M. *et al.* Enhancer-associated H3K4 monomethylation by  
819 Trithorax-related, the Drosophila homolog of mammalian Mll3/Mll4.  
820 *Genes & Development* **26**, 2604–2620 (2012).
- 821 30. Wang, P. *et al.* Global Analysis of H3K4 Methylation Defines MLL  
822 Family Member Targets and Points to a Role for MLL1-Mediated H3K4  
823 Methylation in the Regulation of Transcriptional Initiation by RNA  
824 Polymerase II. *Molecular and Cellular Biology* **29**, 6074–6085 (2009).
- 825 31. Hu, D. *et al.* The MLL3/MLL4 Branches of the COMPASS Family  
826 Function as Major Histone H3K4 Monomethylases at Enhancers.  
827 *Molecular and Cellular Biology* **33**, 4745–4754 (2013).
- 828 32. Lee, J. *et al.* A tumor suppressive coactivator complex of p53 containing  
829 ASC-2 and histone H3-lysine-4 methyltransferase MLL3 or its paralogue  
830 MLL4. *Proc. Natl. Acad. Sci. U.S.A.* **106**, 8513–8518 (2009).
- 831 33. Sedkov, Y. *et al.* Methylation at lysine 4 of histone H3 in ecdysone-  
832 dependent development of Drosophila. *Nature* **426**, 78–83 (2003).
- 833 34. Cheng, J. *et al.* A Role for H3K4 Monomethylation in Gene Repression  
834 and Partitioning of Chromatin Readers. *Molecular Cell* **53**, 979–992  
835 (2014).
- 836 35. Chauhan, C., Zraly, C. B., Parilla, M., Diaz, M. O. & Dingwall, A. K.  
837 Histone recognition and nuclear receptor co-activator functions of  
838 Drosophila Cara Mitad, a homolog of the N-terminal portion of  
839 mammalian MLL2 and MLL3. *Development* **139**, 1997–2008 (2012).
- 840 36. Hubert, A. *et al.* Epigenetic regulation of planarian stem cells by the  
841 SET1/MLL family of histone methyltransferases. *Epigenetics* **8**, 79–91  
842 (2013).
- 843 37. Duncan, E. M., Chitsazan, A. D., Seidel, C. W. & Alvarado, A. S. Set1  
844 and MLL1/2 Target Distinct Sets of Functionally Different Genomic Loci  
845 In Vivo. *CellReports* **13**, 2741–2755 (2015).
- 846 38. Lee, J.-E. *et al.* H3K4 mono- and di-methyltransferase MLL4 is required  
847 for enhancer activation during cell differentiation. *eLife* **2**, 2817–25  
848 (2013).
- 849 39. Mohan, M. *et al.* The COMPASS Family of H3K4 Methylases in  
850 Drosophila. *Molecular and Cellular Biology* **31**, 4310–4318 (2011).
- 851 40. Wang, C. *et al.* Enhancer priming by H3K4 methyltransferase MLL4

- 852 controls cell fate transition. *Proc. Natl. Acad. Sci. U.S.A.* **113**, 11871–  
853 11876 (2016).
- 854 41. Denissov, S. *et al.* Mll2 is required for H3K4 trimethylation on bivalent  
855 promoters in embryonic stem cells, whereas Mll1 is redundant.  
856 *Development* **141**, 526–537 (2014).
- 857 42. Hsieh, J. J.-D., Ernst, P., Erdjument-Bromage, H., Tempst, P. &  
858 Korsmeyer, S. J. Proteolytic cleavage of MLL generates a complex of  
859 N- and C-terminal fragments that confers protein stability and  
860 subnuclear localization. *Molecular and Cellular Biology* **23**, 186–194  
861 (2003).
- 862 43. Chen, W. *et al.* Malignant Transformation Initiated by Mll-AF9: Gene  
863 Dosage and Critical Target Cells. *Cancer Cell* **13**, 432–440 (2008).
- 864 44. Corral, J. *et al.* An Mll-AF9 fusion gene made by homologous  
865 recombination causes acute leukemia in chimeric mice: a method to  
866 create fusion oncogenes. *Cell* **85**, 853–861 (1996).
- 867 45. Thirman, M. J. *et al.* Rearrangement of the MLL gene in acute  
868 lymphoblastic and acute myeloid leukemias with 11q23 chromosomal  
869 translocations. *N. Engl. J. Med.* **329**, 909–914 (1993).
- 870 46. Sobulo, O. M. *et al.* MLL is fused to CBP, a histone acetyltransferase, in  
871 therapy-related acute myeloid leukemia with a t(11;16)(q23;p13.3). *Proc*  
872 *Natl Acad Sci USA* **94**, 8732–8737 (1997).
- 873 47. Goo, Y. H. *et al.* Activating Signal Cointegrator 2 Belongs to a Novel  
874 Steady-State Complex That Contains a Subset of Trithorax Group  
875 Proteins. *Molecular and Cellular Biology* **23**, 140–149 (2003).
- 876 48. Lee, S. *et al.* Coactivator as a target gene specificity determinant for  
877 histone H3 lysine 4 methyltransferases. *Proc Natl Acad Sci USA* **103**,  
878 15392–15397 (2006).
- 879 49. Bienz, M. The PHD finger, a nuclear protein-interaction domain. *Trends*  
880 *in Biochemical Sciences* **31**, 35–40 (2006).
- 881 50. Lee, S., Lee, J., Lee, S.-K. & Lee, J. W. Activating Signal Cointegrator-2  
882 Is an Essential Adaptor to Recruit Histone H3 Lysine 4  
883 Methyltransferases MLL3 and MLL4 to the Liver X Receptors. *Molecular*  
884 *Endocrinology* **22**, 1312–1319 (2008).
- 885 51. Ansari, K. I., Hussain, I., Kasiri, S. & Mandal, S. S. HOXC10 is  
886 overexpressed in breast cancer and transcriptionally regulated by  
887 estrogen via involvement of histone methylases MLL3 and MLL4.  
888 *Journal of Molecular Endocrinology* **48**, 61–75 (2012).
- 889 52. Guo, T., Peters, A. H. F. M. & Newmark, P. A. A bruno-like Gene Is  
890 Required for Stem Cell Maintenance in Planarians. *Developmental Cell*  
891 **11**, 159–169 (2006).
- 892 53. Wenemoser, D. & Reddien, P. W. Planarian regeneration involves  
893 distinct stem cell responses to wounds and tissue absence.  
894 *Developmental Biology* **344**, 979–991 (2010).
- 895 54. Currie, K. W. & Pearson, B. J. Transcription factors *lhx1/5-1* and *pitx* are  
896 required for the maintenance and regeneration of serotonergic neurons  
897 in planarians. *Development* **140**, 3577–3588 (2013).
- 898 55. Oviedo, N. J., Pearson, B. J., Levin, M. & Sanchez Alvarado, A.  
899 Planarian PTEN homologs regulate stem cells and regeneration through  
900 TOR signaling. *Disease Models and Mechanisms* **1**, 131–143 (2008).
- 901 56. Gonzalez-Estevez, C. *et al.* SMG-1 and mTORC1 Act Antagonistically

- 902 to Regulate Response to Injury and Growth in Planarians. *PLoS Genet*  
903 **8**, e1002619–17 (2012).
- 904 57. van Wolfswinkel, J. C., Wagner, D. E. & Reddien, P. W. Single-Cell  
905 Analysis Reveals Functionally Distinct Classes within the Planarian  
906 Stem Cell Compartment. *Stem Cell* **15**, 326–339 (2014).
- 907 58. Zink, D., Fische, A. H. & Nickerson, J. A. Nuclear structure in cancer  
908 cells. *Nat Rev Cancer* **4**, 677–687 (2004).
- 909 59. Kim, D.-H., Kim, J. & Lee, J. W. Requirement for MLL3 in p53  
910 Regulation of Hepatic Expression of Small Heterodimer Partner and Bile  
911 Acid Homeostasis. *Molecular Endocrinology* **25**, 2076–2083 (2011).
- 912 60. Lee, M. G. *et al.* Demethylation of H3K27 regulates polycomb  
913 recruitment and H2A ubiquitination. *Science* **318**, 447–450 (2007).
- 914 61. Pearson, B. J. & Alvarado, A. S. A planarian p53 homolog regulates  
915 proliferation and self-renewal in adult stem cell lineages. *Development*  
916 **137**, 213–221 (2009).
- 917 62. März, M., Seebeck, F. & Bartscherer, K. A Pitx transcription factor  
918 controls the establishment and maintenance of the serotonergic lineage  
919 in planarians. *Development* **140**, 4499–4509 (2013).
- 920 63. Pomeroy, S. L. *et al.* Prediction of central nervous system embryonal  
921 tumour outcome based on gene expression. *Nature* **415**, 436–442  
922 (2002).
- 923 64. Roh, M. *et al.* Overexpression of the oncogenic kinase Pim-1 leads to  
924 genomic instability. *Cancer Res* **63**, 8079–8084 (2003).
- 925 65. Valdman, A., Fang, X., Pang, S.-T., Ekman, P. & Egevad, L. Pim-1  
926 expression in prostatic intraepithelial neoplasia and human prostate  
927 cancer. *Prostate* **60**, 367–371 (2004).
- 928 66. Shirogane, T. *et al.* Synergistic roles for Pim-1 and c-Myc in STAT3-  
929 mediated cell cycle progression and antiapoptosis. *Immunity* **11**, 709–  
930 719 (1999).
- 931 67. Kim, J.-H. *et al.* UTX and MLL4 Coordinately Regulate Transcriptional  
932 Programs for Cell Proliferation and Invasiveness in Breast Cancer Cells.  
933 *Cancer Res* **74**, 1705–1717 (2014).
- 934 68. Zhang, Z. *et al.* Mammary-Stem-Cell-Based Somatic Mouse Models  
935 Reveal Breast Cancer Drivers Causing Cell Fate Dysregulation.  
936 *CellReports* **16**, 3146–3156 (2016).
- 937 69. Reya, T., Morrison, S. J., Clarke, M. F. & Weissman, I. L. Stem cells,  
938 cancer, and cancer stem cells. *Nature* **414**, 105–111 (2001).
- 939 70. Dean, M., Fojo, T. & Bates, S. Tumour stem cells and drug resistance.  
940 *Nat Rev Cancer* **5**, 275–284 (2005).
- 941 71. Cho, Y. W. *et al.* PTIP Associates with MLL3- and MLL4-containing  
942 Histone H3 Lysine 4 Methyltransferase Complex. *Journal of Biological*  
943 *Chemistry* **282**, 20395–20406 (2007).
- 944 72. Cebria, F. Planarian homologs of netrin and netrin receptor are required  
945 for proper regeneration of the central nervous system and the  
946 maintenance of nervous system architecture. *Development* **132**, 3691–  
947 3703 (2005).
- 948 73. Gonzalez-Estevéz, C., Arseni, V., Thambyrajah, R. S., Felix, D. A. &  
949 Aboobaker, A. A. Diverse miRNA spatial expression patterns suggest  
950 important roles in homeostasis and regeneration in planarians. *Int. J.*  
951 *Dev. Biol.* **53**, 493–505 (2009).

- 952 74. Cebria, F. & Newmark, P. A. Morphogenesis defects are associated  
953 with abnormal nervous system regeneration following roboA RNAi  
954 in planarians. *Development* **134**, 833–837 (2007).  
955 75. Romero, B. T., Evans, D. J. & Aboobaker, A. A. in *Progenitor Cells* **916**,  
956 167–179 (Humana Press, 2012).  
957 76. Bolger, A. M., Lohse, M. & Usadel, B. Trimmomatic: a flexible trimmer  
958 for Illumina sequence data. *Bioinformatics* **30**, 2114–2120 (2014).  
959 77. Robb, S. M. C., Gotting, K., Ross, E. & Sánchez Alvarado, A. SmedGD  
960 2.0: The Schmidtea mediterranea genome database. *Genesis* **53**, 535–  
961 546 (2015).  
962 78. Attrill, H. *et al.* FlyBase: establishing a Gene Group resource for  
963 *Drosophila melanogaster*. *Nucleic Acids Research* **44**, D786–92 (2016).  
964 79. Orlando, D. A. *et al.* Quantitative ChIP-Seq Normalization Reveals  
965 Global Modulation of the Epigenome. *CellReports* **9**, 1163–1170 (2014).  
966 80. Bray, N. L., Pimentel, H., Melsted, P. & Pachter, L. Near-optimal  
967 probabilistic RNA-seq quantification. *Nat Biotech* **34**, 525–527 (2016).  
968 81. Pimentel, H. J., Bray, N., Puente, S., Melsted, P. & Pachter, L.  
969 Differential analysis of RNA-Seq incorporating quantification  
970 uncertainty. (2016). doi:10.1101/058164  
971 82. Pimentel, H. J., Bray, N., Puente, S., Melsted, P. & Pachter, L.  
972 Differential analysis of RNA-Seq incorporating quantification  
973 uncertainty. (2016). doi:10.1101/058164  
974

975

976

## 977 **Figure legends**

978 **Figure 1. *S. mediterranea* has three partial *Mll3/4* orthologs expressed in**  
979 **stem cells. (a)** A schematic depicting the structure and domain composition  
980 of MLL3/MLL4 proteins in *D. melanogaster*, *H. sapiens* and *S. mediterranea*.  
981 **(b)** *Mll3/4* genes' expression pattern in wildtype (WT) and two days following a  
982 lethal dose (60 Gy) of gamma irradiation (PI = post-irradiation). *Porcupine-1*  
983 (expressed in the irradiation-insensitive cells of the differentiated gut) and  
984 *H2B* (expressed in the irradiation-sensitive neoblasts) are used as a negative  
985 and positive control respectively. Ten worms per condition were used. **(c)**  
986 White arrows point to examples of cells double-positive for *Mll3/4* transcripts  
987 and *H2B* transcripts. The schematic shows the body area imaged. **(d)** Graph  
988 showing the raw cell counts used for percentage estimates in **(c)**. Green  
989 colour represents all counted *H2B*-positive cells, yellow represents *H2B*-  
990 positive cells also expressing a *Mll3/4* ortholog. Error bars represent Standard  
991 Error of the Mean (SEM). Ten animals per condition were used. **(e)**

992 Expression profiles of *Mll3/4* genes according to RNA-seq data from FACS-  
993 sorted X1 (stem cells in G2/M phase), X2 (stem cells in G1 and stem cell  
994 progeny) and X ins (differentiated cells) planarian cell populations.

995

996

997 **Figure 2. *LPT*(RNAi) results in differentiation defects and outgrowth**  
998 **formation during regeneration. (a)** A schematic showing the amputation of  
999 RNAi worms into head (H), middle (M) and tail (T) pieces in order to observe  
1000 regeneration of different structures. The time-course of all the experiments on  
1001 *Mll3/4* knockdown animals is depicted underneath the worm schematic. A  
1002 total of 9 days of dsRNA microinjection-mediated RNAi was followed by  
1003 amputation on the 10<sup>th</sup> day and subsequent observation of regeneration. **(b)**  
1004 Head, middle and tail pieces following *LPT*(RNAi) or control *GFP*(RNAi) at  
1005 day 8 of regeneration. Yellow arrows point towards the smaller blastema and  
1006 the eye formation defects. **(c)** Head, middle and tail pieces following  
1007 *LPT*(RNAi) or control *GFP*(RNAi) at day 10 of regeneration. Red arrows point  
1008 towards outgrowths. **(d)** Head, middle and tail pieces following *LPT*(RNAi) or  
1009 control *GFP*(RNAi) at day 14 of regeneration. Red arrows point towards  
1010 outgrowths. **(e)** Gut regeneration and maintenance in middle pieces following  
1011 *LPT*(RNAi), as illustrated by RNA probe for the gene *porcupine-1* at 8 days of  
1012 regeneration. **(f)** Brain regeneration in middle pieces at 8 days post-  
1013 amputation following *LPT*(RNAi), as illustrated by anti-SYNORF-1 antibody  
1014 labeling the central nervous system (CNS). **(g)** Optic chiasma recovery in tail  
1015 pieces at 8 days of regeneration following *LPT*(RNAi), as shown by anti-VC-1  
1016 antibody. **(h)** Recovery of optic cups and organized trail of optic cup precursor  
1017 cells in tail pieces at 8 days of regeneration following *LPT*(RNAi), as  
1018 demonstrated by RNA probe for *SP6-9*. **(i)** Pharynx recovery in head pieces at  
1019 8 days of regeneration following *LPT*(RNAi), as illustrated by RNA probe for  
1020 *laminin*. Images in **(e,f, i)** are representative of two separate experiments  
1021 using 10 animals per condition each. Images in **(g, h)** were obtained from one  
1022 experiment each, using 10 animals per condition. Numbers at the top right of  
1023 each regenerating piece represent number of animals in the condition  
1024 showing the same phenotypic features as the animal in the panel.

1025

1026

1027 **Figure 3. LPT controls differentiation across neuronal and epidermal**  
1028 **lineages.** Quantification of the number of GABAergic neurons (labeled by  
1029 *GAD*) (**a**), dopaminergic neurons (labeled by *TH*) (**b**), acetylcholinergic  
1030 neurons (labeled by *chat*) (**c**), serotonergic neurons (labeled by *TPH*) (**d**) and  
1031 early (labeled by *NB.21.11e*) and late (labeled by *AGAT-1*) epidermal stem  
1032 cell progeny (**e**) at 8 days of regeneration of tail or middle pieces following  
1033 *LPT*(RNAi). For each of the comparisons in this figure a 2-tailed ttest  
1034 assuming unequal variance was used; a single asterisk indicates  $p < 0.05$ ,  
1035 while three asterisks indicate  $p < 0.001$ . Error bars represent Standard Error of  
1036 the Mean (SEM). Ten animals per condition per experiment were assessed  
1037 over the course of two separate experiments.

1038

1039

1040 **Figure 4. Over-proliferation and mitotic cell clustering precedes and**  
1041 **accompanies the emergence of outgrowths in *LPT*(RNAi) regenerating**  
1042 **animals.** (**a**) Quantification of mitotic cell numbers (mitotic cells labeled by  
1043 anti-H3P antibody) at different post-amputation timepoints following  
1044 *LPT*(RNAi). The figure is a representative of three repeats of the same  
1045 experiment, each using 10 animals per timepoint. The statistical test used was  
1046 a 2-tailed ttest assuming unequal variance. The asterisks indicate  $p < 0.05$ .  
1047 Error bars represent Standard Error of the Mean (SEM). (**b**) Examples of  
1048 middle pieces at the timepoints post-amputation showing significant difference  
1049 in mitotic cell counts according to (**a**). ‘ph’ indicates where the pharynx is in  
1050 each piece. The red arrows point towards clusters of mitotic cells in late stage  
1051 regenerates (192 hrs/8 days). (**c**) Brightfield examples of middle pieces  
1052 forming outgrowths at timepoints after the observation of mitotic clusters in  
1053 (**b**). Red arrows point towards outgrowths. (**d**) *LPT*(RNAi) head pieces that do  
1054 not contain an outgrowth, but show mitotic cell clusters (indicated by yellow  
1055 arrows). One piece shows staining in the eye region, which is an artifact of the  
1056 procedure. The lower panel shows a mitotic cell at the border of an outgrowth  
1057 and the body in a head piece at 10 days of regeneration following *LPT*(RNAi).  
1058 Red arrow points towards the outgrowth and yellow arrow points towards the  
1059 mitotic cell. (**e**) An example of a tail piece at 12 days of regeneration having a

1060 mitotic cell-rich cephalic outgrowth following *LPT*(RNAi). Yellow arrows show  
1061 the mitotic cells in the outgrowth.

1062

1063

1064 **Figure 5. Stem cells at different stages of commitment are found in**  
1065 **outgrowths of *LPT*(RNAi) regenerating animals.** (a) A head piece at 18  
1066 days of regeneration following *LPT*(RNAi) showing *sigma* stem cells in its  
1067 posterior outgrowth. *Sigma* stem cells are double positive for *Smedwi-1* and  
1068 the '*sigma pool*' of RNA probes (*Soxp1*, *Soxp2*). Red arrows in the brightfield  
1069 images panel point towards the outgrowths and white arrows in the zoomed-in  
1070 panel show a double-positive cell and a *Smedwi-1* single-positive cell. (b) A  
1071 head piece at 10 days of regeneration following *LPT*(RNAi) showing *zeta*  
1072 stem cells in its posterior outgrowth. *Zeta* stem cells are double positive for  
1073 *Smedwi-1* and the '*zeta pool*' of RNA probes (*zfp-1*, *Soxp3*, *egr-1*). The red  
1074 arrow in the brightfield images panel points towards the outgrowth and the  
1075 white arrows in the zoomed-in panel show double-positive cells. (c) A middle  
1076 piece at 11 days of regeneration following *LPT*(RNAi) showing *gamma* stem  
1077 cells in its lateral outgrowth. *Gamma* stem cells are double positive for  
1078 *Smedwi-1* and the '*gamma pool*' of RNA probes (*gata4/5/6*, *hnf4*). The red  
1079 arrow in the brightfield images panel points towards the outgrowth and the  
1080 white arrows in the zoomed-in panel show a double-positive cell, a *Smedwi-1*  
1081 single-positive cell and a *gamma pool* single-positive cell. In (a), (b) and (c)  
1082 the normal tissue margin is shown via white dashed lines.

1083

1084

1085 **Figure 6. *LPT*(RNAi) results in a cancer-like phenotype.** A summary of the  
1086 differentiation and neoblast proliferation data presented, together with a  
1087 simplified flowchart illustrating the tested lineages' development under  
1088 knockdown conditions. A red cross sign indicates where the defect in a  
1089 lineage is detected following *LPT*(RNAi).

1090

1091

1092 **Figure 7. RNA-seq of G2/M stem cells following *LPT*(RNAi) reveals**  
1093 **effects on genes enriched in different cell populations.** (a) Genes were



1094 classified according to their proportional expression in the X1 (G2/M stem  
1095 cells; dark blue), X2 (G1 stem cells and stem cell progeny; light blue) and X  
1096 ins (differentiated cells; orange) FACS populations of cells. Genes were  
1097 defined as enriched in certain population(s) if more than 50% of their  
1098 expression is observed in that population in wildtype or more than 75% of  
1099 their expression is observed across two cell populations. Genes not enriched  
1100 in either population were classified as 'not enriched'. Each vertical line  
1101 represents a gene. Under the population expression enrichment track is a  
1102 track with all the significantly up- and down-regulated genes in G2/M stem  
1103 cells following *LPT*(RNAi). The genes with fold change  $>1.5$  ( $p < 0.05$ ) are  
1104 shown in red following a log<sub>2</sub> fold change transformation. The genes with fold  
1105 change  $<-1.5$  ( $p < 0.05$ ) are shown in blue following a log<sub>2</sub> fold change  
1106 transformation. The Wald's test (as part of the Sleuth software) was used for  
1107 assessing differential expression. (b) Enrichment for genes in each of the six  
1108 classes was calculated for the up- and down-regulated genes' list (red and  
1109 blue respectively). Enrichment for Transcription Factors (TFs) was also  
1110 performed. The number of genes in each group is indicated in brackets under  
1111 the group's name. Numbers in white represent significant enrichment ( $p < 0.01$ )  
1112 according to a hypergeometric enrichment test. (c) Gene Ontology (GO)  
1113 enrichment analysis on the genes significantly up-regulated (red) and down-  
1114 regulated (blue) in G2/M stem cells following *LPT*(RNAi). Categories are  
1115 sorted by average Log<sub>2</sub> fold change of the up- or down-regulated genes  
1116 falling in each category. In bold are shown terms that relate to the described  
1117 *Mll3/4* loss of function phenotype.

1118

1119

1120 **Figure 8. *LPT*(RNAi) is mainly manifested in changes in H3K4me1 and**  
1121 **H3K4me3 around the TSS in G2/M stem cells.** (a) Graphs presenting the  
1122 average read coverage across the genome for H3K4me3, H3K4me1 and  
1123 H3K27me3 (centered on the TSS, showing 2 kb upstream and downstream)  
1124 normalised to *Drosophila* S2 signal spike-in. The input coverage is subtracted.  
1125 Log<sub>2</sub> fold change graphs are also shown for each histone modification, where  
1126 signal above zero shows increase following *LPT*(RNAi) and signal below zero  
1127 represents a decrease. Three colours are used for different gene classes –

1128 dark blue (genes enriched in G2/M stem cells (X1)), light blue (genes enriched  
1129 in G1 stem cells and stem cell progeny (X2)), orange (genes enriched in  
1130 differentiated cells (X ins)). Standard deviation is shown by a faded colour  
1131 around each line. (b) Spearman's rank correlation between changes in RNA-  
1132 seq signal and H3K4me1 or H3K4me3 ChIP-seq signal for the region around  
1133 the TSS of genes from different enrichment classes (only examples where a  
1134 significant correlation exists are shown). The blue line represents a correlation  
1135 where no filter for fold change in the RNA-seq data was applied. The green  
1136 line shows a correlation where RNA-seq fold change data was filtered for  
1137 Log2 fold changes  $\leq -1$  and  $\geq +1$ . Faded areas of the lines represent results  
1138 not significant at  $p < 0.001$ , while darker colours represent results significant at  
1139  $p < 0.001$ .

1140

1141

1142 **Figure 9. *LPT* regulates the expression of known and putative**  
1143 **oncogenes and tumor suppressors. (a)** Examples of genes significantly  
1144 ( $p < 0.05$ ) mis-regulated in G2/M stem cells following *LPT*(RNAi). RNA-seq fold  
1145 change is shown in red (up-regulation) and blue (down-regulation). The  
1146 genes' enrichment class is also shown. The ChIP-seq profile for H3K4me3 in  
1147 the 2 kb region around the TSS of each gene is presented. Purple colour  
1148 represents normalised signal following *LPT*(RNAi) and green colour is used  
1149 to show the normalised signal following *GFP*(RNAi). 'TF' stands for 'transcription  
1150 factor'. (b) *in silico* analysis ([www.oncomine.org](http://www.oncomine.org); ttest,  $p < 0.0001$ ) of *Mll3* and  
1151 *pitx2* expression in normal tissue (cerebellum) and cancer tissue  
1152 (medulloblastoma). (c) *pitx* and *Smedwi-1* *in situ* hybridization at 8 days of  
1153 regeneration of middle pieces following *LPT*(RNAi). White arrows show  
1154 double-positive cells. Cell counts are compared using a 2-tailed ttest  
1155 assuming unequal variance. The asterisk indicates  $p < 0.05$ . Ten animals per  
1156 condition were used.

1157

1158

1159 **Figure 10. Double knockdown with *utx* or *pim-1-like* alleviates the**  
1160 ***LPT*(RNAi) over-proliferation and outgrowth phenotype. (a)** More  
1161 examples of genes significantly ( $p < 0.05$ ) mis-regulated in G2/M stem cells

1162 following *LPT*(RNAi). RNA-seq fold change is shown in red (up-regulation)  
1163 and blue (down-regulation). The genes' enrichment class is also shown. The  
1164 ChIP-seq profile for a histone modification in the 2 kb region around the TSS  
1165 of each gene is presented. Purple colour represents normalised signal  
1166 following *LPT*(RNAi) and green colour is used to show the normalised signal  
1167 following *GFP*(RNAi). Depending on the gene enrichment class, H3K4me1 or  
1168 H3K4me3 ChIP-seq signal is presented for each gene (based on previous  
1169 Spearman's rank correlation analyses in **Figure 8**). Bold font of a gene name  
1170 illustrates an example where there is a correlation between ChIP-seq and  
1171 RNA-seq data. **(b)** Mean average mitotic cell (labeled by anti-H3P antibody)  
1172 counts at 48 hours post-amputation following double knockdown experiments.  
1173 Ten animals per condition were used. The statistical test used was a 2-tailed  
1174 ttest assuming unequal variance. The asterisks indicate significant differences  
1175 at  $p < 0.05$ . Error bars represent Standard Error of the Mean (SEM).  
1176 Representative tail piece examples are shown for each condition significantly  
1177 different from the control *GFP/GFP*(RNAi) animals or from the  
1178 *GFP/LPT*(RNAi) condition. **(c)** Percentage quantification of double knockdown  
1179 regenerates developing outgrowths.

1180

## 1181 **Additional File Legends**

1182

1183 **Additional File 1 (PDF) Structure and function of COMPASS and**  
1184 **COMPASS-like core proteins.** **(a)** Schematics of the core subunits of the  
1185 COMPASS and the two COMPASS-like complexes in mammals are  
1186 presented with coloured boxes corresponding to different protein domains –  
1187 RRM1 (RNA-recognition motif), N-SET, SET, CXXC (zinc finger), PHD (Plant  
1188 Homeodomain fingers), zf (PHD-like zinc finger), FYRN  
1189 (Phenylalanine/Tyrosine rich N-terminus domain), FYRC  
1190 (Phenylalanine/Tyrosine rich C-terminus domain), purple stars signifying  
1191 nuclear receptor recognition motifs. Dashed vertical line represents proteolytic  
1192 cleavage. **(b)** As in **(a)**, but in fruitfly. **(c)** Proposed mechanisms of action of  
1193 each core complex subunit. COMPASS complex – 1) performing H3K4  
1194 trimethylation on TSS of most actively transcribed genes and 2) depositing

1195 H3K4me2 on the gene bodies of actively transcribed genes. MLL1/2/Trithorax  
1196 COMPASS-like complex – 1) a role in transcriptional activation of Hox genes  
1197 via trimethylating H3K4 on TSS of their promoters and 2) MLL2 is involved in  
1198 trimethylation of H3K4 on TSS of bivalent promoters. MLL3/4/LPT/Trr – 1) role  
1199 in hormone-dependent transcription – when the Nuclear Receptor protein  
1200 (NR) is bound to the DNA Hormone Response Element (HRE) upon Hormone  
1201 Ligand (HL) detection, MLL3/4/LPT/Trr complex binds the nuclear receptor  
1202 and serves as its co-activator via trimethylating H3K4 and promoting active  
1203 transcription on selected loci; 2) a switch between inactive and active  
1204 enhancer states where MLL3/4/LPT/Trr complex deposits H3K4me1 on both  
1205 active and inactive enhancers; upon UTX recruitment, it demethylates  
1206 H3K27me3 and allows for CBP/p300 to acetylate H3K27 and activate the  
1207 enhancer; 3) a switch between active and inactive promoters -  
1208 MLL3/4/LPT/Trr complex bound to TSS deposits H3K4me1 on the TSS and  
1209 around it, leads to repressed transcription of the gene; when H3K4me1 is  
1210 depleted from the TSS and another complex performs trimethylation of H3K4  
1211 on TSS, this is correlated with activated transcription. (d) Schematic  
1212 representation of planarian COMPASS and COMPASS-like core subunits.  
1213 SMED-LPT (in red) is characterized in the present study. (e) Planarian  
1214 COMPASS and COMPASS-like core subunits' expression in the three  
1215 populations of cells sortable by fluorescence-activated cell sorting (FACS)  
1216 (X1=G2/M stem cells, X2=G1 stem cells and stem cell progeny, X  
1217 ins=differentiated cells) according to RNA-seq data. (f) Known defects after  
1218 RNAi-mediated knockdown of core COMPASS and COMPASS-like subunits  
1219 in planarians.

1220

1221

1222 **Additional File 2 (PDF) Planarian *Mll3/4* genes are expressed in**  
1223 **neoblasts and neoblast progeny and colocalise with each other. (a)**  
1224 Protein alignment of conserved regions of COMPASS-like families' core  
1225 proteins. Asterisks indicate complete conservation in all sequences, while  
1226 black boxes are drawn around areas of conservation specific to the  
1227 MLL3/4/Trithorax-related family. Colours represent similarity of amino acids.  
1228 The image was produced using MEGA.5.2 software. (b) *LPT*, *trr-1* and *trr-2*

1229 expression in wildtype and irradiated 3 day-regenerating head and middle  
1230 pieces. Arrows in head pieces point towards expression in the forming  
1231 pharynx, while arrows in middle pieces point towards expression in the  
1232 forming brain. (c) *LPT*, *trr-1* and *trr-2* expression in intact animals following  
1233 *GFP*(RNAi) or following *H2B*(RNAi). *Porcupine-1* and *Smedwi-2* were used as  
1234 a negative and positive control respectively. (d) *LPT*, *trr-1* and *trr-2* co-  
1235 expression in the head region (as shown by the schematics). White arrows  
1236 point towards cells showing colocalisation.

1237

1238

1239 **Additional File 3 (PDF) Phenotype scoring of *Mll3/4* knockdown**  
1240 **planarians during regeneration and homeostasis.** (a) Proportion of head,  
1241 middle and tail regenerates exhibiting particular phenotypic characteristics  
1242 following *LPT*(RNAi), *trr-1*(RNAi) and *trr-2*(RNAi). (b) Survival curves for head,  
1243 middle and tail pieces following *LPT*(RNAi), *trr-1*(RNAi) and *trr-2*(RNAi). (c)  
1244 Proportion of intact (homeostatic) animals with particular phenotypic  
1245 characteristics following *LPT*(RNAi), *trr-1*(RNAi) and *trr-2*(RNAi). (d) Survival  
1246 curves for homeostatic animals following *LPT*(RNAi), *trr-1*(RNAi) and *trr-*  
1247 *2*(RNAi).

1248

1249

1250 **Additional File 4 (PDF) *Trr-1*(RNAi) and *trr-2*(RNAi) lead to mild**  
1251 **differentiation defects during regeneration.** (a) A schematic showing the  
1252 amputation of RNAi worms into head (H), middle (M) and tail (T) pieces in  
1253 order to observe regeneration of different structures. The time-course of the  
1254 experiments on *Mll3/4* knockdown animals is depicted underneath the worm  
1255 schematic. A total of 9 days of dsRNA microinjection-mediated RNAi was  
1256 followed by amputation on the 10<sup>th</sup> day and observation of regeneration. (b)  
1257 Head, middle and tail pieces following *trr-1*(RNAi), *trr-2*(RNAi) or control  
1258 *GFP*(RNAi) at day 8 of regeneration. Yellow arrows point towards the  
1259 regenerative defects – smaller blastema, delayed eye formation or posterior  
1260 bloating. (c) Head, middle and tail pieces following *trr-1*(RNAi), *trr-2*(RNAi) or  
1261 control *GFP*(RNAi) at day 14 of regeneration. (d) Central nervous system  
1262 (CNS) maintenance and recovery at 8 days of middle piece regeneration, as

1263 labeled by CNS-specific anti-SYNORF-1 antibody, following *trr-1*(RNAi) or *trr-*  
1264 *2*(RNAi). (e) Gut maintenance and recovery at 8 days of middle piece  
1265 regeneration, as labeled by *porcupine-1*, following *trr-1*(RNAi) or *trr-2*(RNAi).  
1266 (f) Pharynx recovery at 8 days of head piece regeneration, as labeled by  
1267 *laminin*, following *trr-1*(RNAi) or *trr-2*(RNAi). Numbers at the top of each piece  
1268 represent number of animals in that condition showing the same phenotypic  
1269 features as the animal in the panel.

1270

1271

1272 **Additional File 5 (PDF) *Trr-1/ trr-2* double knockdown results in more**  
1273 **prevalent and accelerated outgrowth formation compared to *LPT*(RNAi).**

1274 (a) Head, middle and tail pieces at 3 days of regeneration following  
1275 *GFP/LPT*(RNAi), *GFP/trr-1*(RNAi), *GFP/trr-2*(RNAi), *trr-1/trr-2*(RNAi) and  
1276 *GFP/GFP*(RNAi). Red arrows point towards outgrowths. (b) Percentage of  
1277 head, middle and tail regenerating pieces developing outgrowths throughout  
1278 their life-time. (c) Survival curves of head, middle and tail regenerating pieces.  
1279 The *GFP/GFP*(RNAi) line overlaps with *GFP/trr-1*(RNAi) and *GFP/ trr-*  
1280 *2*(RNAi). Ten animals per condition were used.

1281

1282

1283 **Additional File 6 (PDF) Number of stem cells and early stem cell progeny**  
1284 **is unchanged following knockdown of *LPT*.** The pre-pharyngeal area of  
1285 middle pieces at 8 days of regeneration was used for this experiment. Stem  
1286 cells are labeled with *H2B* and early neoblast progeny cells are *H2B-*  
1287 *negative/anti-SMEDWI-1* antibody-positive cells. Numbers of stem cells and  
1288 progeny cells between *LPT*(RNAi) animals and controls were not significantly  
1289 different (ns). A 2-tailed ttest assuming unequal variance was used. Ten  
1290 animals per condition were processed.

1291

1292

1293 **Additional File 7 (PDF) *Trr-2*(RNAi) regenerating animals produce less**  
1294 **GABAergic and dopaminergic neurons.** Quantification of the number of  
1295 GABAergic neurons (labeled by *GAD*) (a), dopaminergic neurons (labeled by  
1296 *TH*) (b), serotonergic neurons (labeled by *TPH*) (c), acetylcholinergic neurons

1297 (labeled by *chat*) (**d**) and early (labeled by *NB.21.11e*) and late (labeled by  
1298 *AGAT-1*) epidermal stem cell progeny (**e**) at 8 days of regeneration of tail or  
1299 middle pieces following *trr-1*(RNAi) or *trr-2*(RNAi). For each of the  
1300 comparisons in this figure a 2-tailed ttest assuming unequal variance was  
1301 used; a single asterisk indicates  $p < 0.05$ . Error bars represent Standard Error  
1302 of the Mean (SEM). Ten animals per condition per experiment were assessed  
1303 over the course of two separate experiments.

1304

1305

1306 **Additional File 8. (PDF) Tubule-associated protonephridia and cilia cell**  
1307 **regeneration is not affected by *MII3/4* knockdown.** (a) Recovery of dorsal  
1308 and ventral cilia in middle pieces at 8 days of regeneration following  
1309 *LPT*(RNAi), *trr-1*(RNAi) or *trr-2*(RNAi), as labeled by anti-acetylated tubulin  
1310 antibody. (b) Recovery and maintenance of tubule-associated protonephridia  
1311 cells (labeled by *CAVII-1*) in middle pieces at 8 days of regeneration following  
1312 *LPT*(RNAi), *trr-1*(RNAi) or *trr-2*(RNAi). The white dashed line indicates where  
1313 the anterior regenerated body parts following amputation should be. The  
1314 graph compares numbers of *CAVII-1*-positive cells in the newly recovered  
1315 regions, as well as in the whole body, between *MII3/4* genes knockdown  
1316 conditions and controls. For each of the comparisons in this figure a 2-tailed  
1317 ttest assuming unequal variance was used; 'ns' stands for 'not significant'.  
1318 Error bars represent Standard Error of the Mean (SEM). Ten animals per  
1319 condition were used.

1320

1321

1322 **Additional File 9. (PDF) 'Inchworming' following *MII3/4* knockdown is**  
1323 **due to serotonin deficiency.** Locomotive defects in *MII3/4* knockdown  
1324 animals are shown. The number of regenerating head pieces per condition  
1325 exhibiting the respective locomotive defect before and after 45-minute-long  
1326 serotonin hydrochloride treatment is shown in a table. Movie still shots are  
1327 shown for worms in each treatment. There was one-second interval between  
1328 the chosen still shots. The dashed line indicates the locomotive progress that  
1329 the worm had achieved in 3 seconds (from first to last shot). Steeper line  
1330 indicates faster movement. White numbers at the bottom right corners

1331 represent number of animals per condition showing the illustrated behaviour.

1332 Ten animals per condition were used.

1333

1334 **Additional File 10. (PDF) *MII3/4* knockdown leads to changes in mitotic**  
1335 **activity during regeneration and homeostasis. (a)** Mitotic cell number  
1336 fluctuations during regeneration following *trr-1*(RNAi), *trr-2*(RNAi) and  
1337 *GFP*(RNAi). **(b)** Mitotic cell number fluctuations during homeostatic  
1338 observations following *LPT*(RNAi), *trr-1*(RNAi), *trr-2*(RNAi) and *GFP*(RNAi).  
1339 For each of the comparisons in this figure a 2-tailed ttest assuming unequal  
1340 variance was used; a single asterisk indicates  $p < 0.05$ . Error bars represent  
1341 Standard Error of the Mean (SEM). Ten animals per condition were assessed.

1342

1343 **Additional File 11. (PDF) Non-mitotic stem cells are present in**  
1344 **outgrowths of animals following *LPT*(RNAi).** A head piece (containing  
1345 outgrowths) at 10 days of regeneration following *LPT*(RNAi) stained with *H2B*  
1346 RNA probe and anti-H3P mitotic cell antibody. Stem cells found outside the  
1347 usual stem cell compartment are indicated via white arrows. The border of the  
1348 usual neoblast compartment is indicated with a white dashed line.

1349

1350 **Additional File 12. (PDF) *Sigma*, *zeta* and *gamma* neoblast numbers are**  
1351 **unchanged following *LPT*(RNAi). (a, d)** Cells in pre-pharyngeal regions of  
1352 middle pieces at 8 days of regeneration following *LPT*(RNAi) labeled by the  
1353 *sigma pool* of RNA probes (*Soxp1*, *Soxp2*) and *Smedwi-1*. White arrows point  
1354 towards *sigma* neoblasts (double-positive for *sigma pool* and *Smedwi-1*). **(b,**  
1355 **e)** Cells in pre-pharyngeal regions of middle pieces at 8 days of regeneration  
1356 following *LPT*(RNAi) labeled by the *zeta pool* of RNA probes (*zfp-1*, *Soxp3*,  
1357 *egr-1*) and *Smedwi-1*. White arrows point towards *zeta* neoblasts (double-  
1358 positive for *zeta pool* and *Smedwi-1*). **(c, f)** Cells in pre-pharyngeal regions of  
1359 middle pieces at 8 days of regeneration following *LPT*(RNAi) labeled by the  
1360 *gamma pool* of RNA probes (*gata4/5/6*, *hnf4*) and *Smedwi-1*. White arrows



1361 point towards *gamma* neoblasts (double-positive for *gamma pool* and  
1362 *Smedwi-1*). (g) Overall number of *Smedwi-1*-positive cells (regardless of  
1363 colocalisation with other markers) in the pre-pharyngeal region of middle  
1364 pieces at 8 days of regeneration following *LPT*(RNAi). The statistical  
1365 comparisons in this figure were performed via 2-tailed ttest assuming unequal  
1366 variance. 'ns' stands for 'not significant'. Ten worms per condition were  
1367 processed.

1368

1369 **Additional File 13. (PDF) *LPT*(RNAi) results in disorganized outgrowth-**  
1370 **focused expression of epidermal precursor markers, epithelial disarray**  
1371 **and hypertrophy and changes of nuclear morphology.** (a) Anterior part  
1372 (containing an outgrowth) of a tail piece at 18 days of regeneration following  
1373 *LPT*(RNAi) labeled with *NB.21.11e* and *AGAT-1* epidermal precursor markers.  
1374 'CG' stands for 'cephalic ganglia'. (b) The epidermal layer (stained with  
1375 Hoechst 33342) of a tail piece at 10 days of regeneration following *LPT*(RNAi)  
1376 compared to control (c) The nuclear area of 20 epithelial cells per  
1377 experimental and control condition was compared via 2-tailed ttest assuming  
1378 unequal variance. Triple asterisk indicates  $p < 0.001$ . (d) Nuclear morphology  
1379 comparison between a 10-day *LPT*(RNAi) and control regenerate. Samples  
1380 were stained with Hoechst 33342. Yellow arrows point towards misshapen  
1381 nuclei.

1382

1383 **Additional File 14. (PDF) Histone modification ChIP-seq profiles at**  
1384 **promoter-proximal regions of different classes of genes.** (a), (b) and (c)  
1385 show histone modification patterns for H3K4me3, H3K4me1 and H3K27me3  
1386 respectively. ChIP-seq signal is shown in black. Six groups of genes are  
1387 presented – enriched >50% in X1 (G2/M stem cells) shown by dark blue,  
1388 enriched >50% in X2 (G1 stem cells and stem cell progeny) shown in light  
1389 blue, enriched >50% in X ins (differentiated cells) shown in orange, genes  
1390 enriched >75% in X1/X2, >75% in X2/X ins and 'not enriched'. Histone  
1391 modification graphs are centered on the Transcriptional Start Site (TSS) with

1392 2.5 kb shown upstream and downstream.

1393

1394 **Additional File 15. (PDF) The expression of stem cell-enriched genes**  
1395 **mis-regulated following *LPT*(RNAi) is inversely correlated with H3K4me1**  
1396 **TSS-proximal levels. (a)** Graphs presenting the average read coverage  
1397 across the genome for H3K4me3, H3K4me1 and H3K27me3 (centered on the  
1398 TSS, showing 2 kb upstream and downstream) normalised to *Drosophila* S2  
1399 signal spike-in. The input coverage is subtracted. Log2 fold change graphs  
1400 are also shown for each histone modification, where signal above zero shows  
1401 increase following *LPT*(RNAi) and signal below zero represents a decrease.  
1402 Three colours are used for different gene classes – green (genes enriched in  
1403 X1/X2 cells), red (genes enriched in X2/X ins cells), black (genes not enriched  
1404 in any population of cells). Standard deviation is shown as a faded colour  
1405 around each line. **(b)** Log2 fold change of signal around the TSS across  
1406 different histone marks and gene classes following *LPT*(RNAi). Blue  
1407 represents genes down-regulated following *LPT*(RNAi) and red – up-  
1408 regulated. Standard deviation is shown by a faded colour around each line.  
1409

1410 **Additional File 16. (PDF) *LPT* regulates the expression of cancer- and**  
1411 **development-associated genes.** Examples of genes significantly ( $p < 0.05$ )  
1412 mis-regulated in G2/M stem cells following *LPT*(RNAi). RNA-seq fold change  
1413 is shown in red (up-regulation) and blue (down-regulation). The genes'  
1414 enrichment class is also shown. The ChIP-seq profile for a histone  
1415 modification in the 2 kb region around the TSS of each gene is presented.  
1416 Purple colour represents normalised signal following *LPT*(RNAi) and green  
1417 colour is used to show the normalised signal following *GFP*(RNAi). Depending  
1418 on the gene enrichment class, H3K4me1 **(a)** or H3K4me3 **(b)** ChIP-seq signal  
1419 is presented for each gene (based on previous Spearman's rank correlation  
1420 analyses in **Figure 8**). Bold font of a gene name illustrates an example where  
1421 there is a correlation between ChIP-seq and RNA-seq data. 'TF' stands for  
1422 'transcription factor'.

1423

1424 **Additional File 17. (PDF) Phenotype scoring of double knockdown**  
1425 **(*GFP/LPT*, *GFP/pim-1*, *GFP/pim-1-like*, *GFP/utx*, *pim-1/pim-1-like*,**  
1426 ***LPT/pim-1*, *LPT/pim-1-like*, *LPT/utx* and *GFP/GFP*) planarians during**  
1427 **regeneration.** Proportion of head, middle and tail regenerates exhibiting  
1428 particular phenotypic characteristics following a double knockdown. The  
1429 proportion of animals forming outgrowths is given regardless of regenerating  
1430 piece identity.

1431

1432 **Additional File 18. (PDF) The histone modifications antibodies used for**  
1433 **ChIP-seq experiments are specific.** (a) Western blot with loading control  
1434 anti-H3 (unmodified histone H3) and anti-H3K4me1 on whole animal protein  
1435 lysate from *GFP*(RNAi) and *LPT*(RNAi) samples. (b) Western blot with loading  
1436 control anti-H3 (unmodified histone H3) and anti-H3K4me3 on whole animal  
1437 protein lysate from *GFP*(RNAi) and *set1*(RNAi) samples. (c) Western blot with  
1438 loading control anti-H3 (unmodified histone H3) and anti-H3K27me3 on whole  
1439 animal protein lysate from *GFP*(RNAi) and *utx*(RNAi) samples.

1440

1441 **Additional file19. (PDF) Summary of planarian ChIP-seq procedure.**  
1442 Three day-regenerating planarians were dissociated into single cells. Cells  
1443 were stained with Hoechst 34580 and Calcein AM in order to visualize cell  
1444 populations according to nuclear size and cytoplasmic complexity. The X1  
1445 (G2/M) stem cells (magenta) were sorted and mixed with 4% *Drosophila* S2  
1446 cells. Cells were crosslinked with 1% Formaldehyde and sonicated.  
1447 Immunoprecipitation with anti-H3K4me3, anti-H3K4me1 and anti-H3K27me3  
1448 antibodies followed. Samples were reverse-crosslinked and libraries were  
1449 prepared using NEBNext Ultra II library preparation kit.

1450

1451 **Additional File 20. (.xlsx) Differentially expressed loci following**

1452 **LPT(RNAi)**. Each row represents one locus that was differentially expressed  
1453 with a p-value less than 0.05 and fold change <-1.5 or >1.5. The Wald's test  
1454 (as part of the Sleuth software) was used for assessing differential  
1455 expression. The top BLAST hit (with e-value) and the common model  
1456 organism top BLAST hit is also provided for each locus.

1457

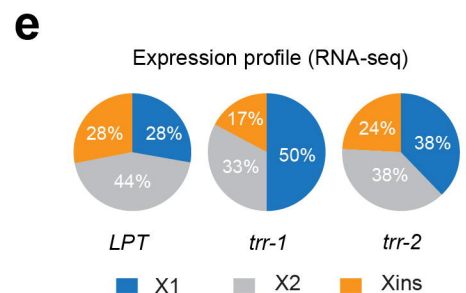
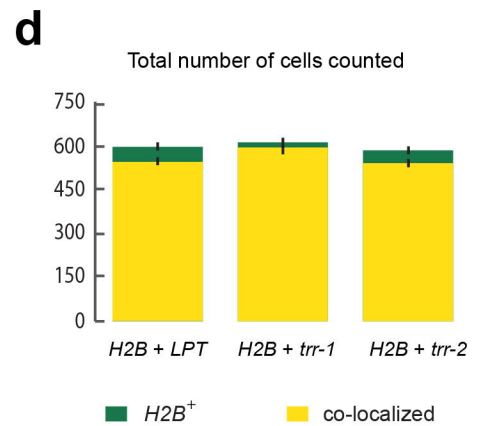
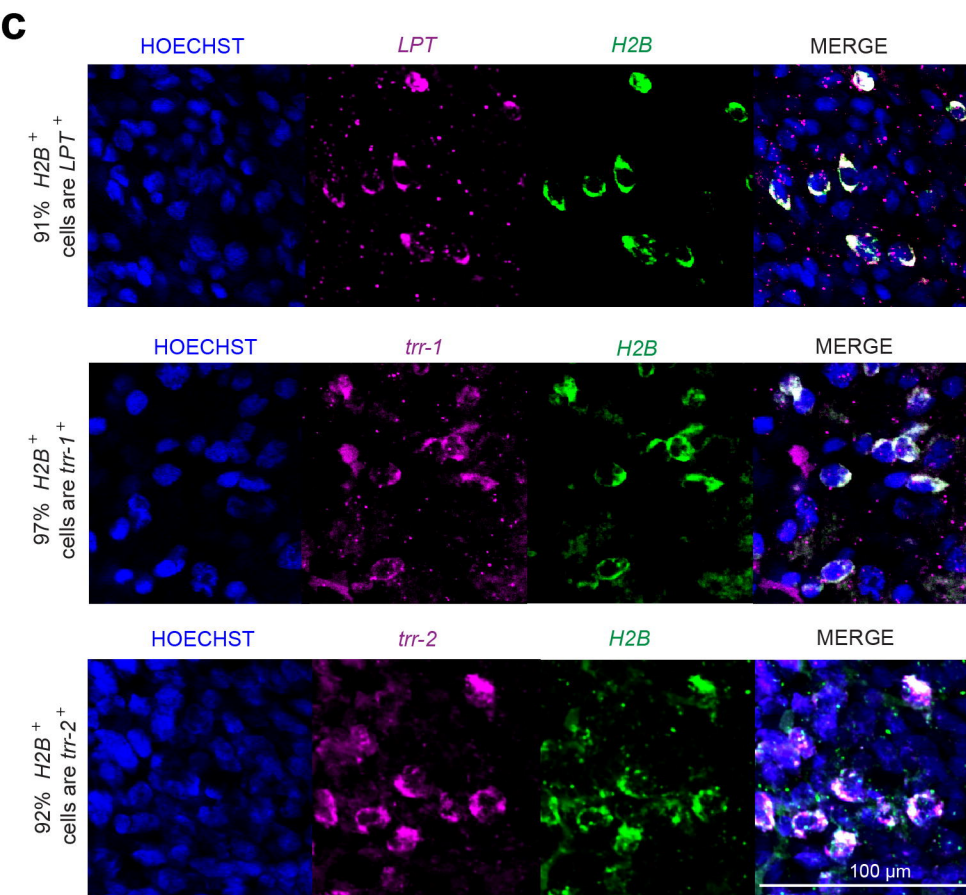
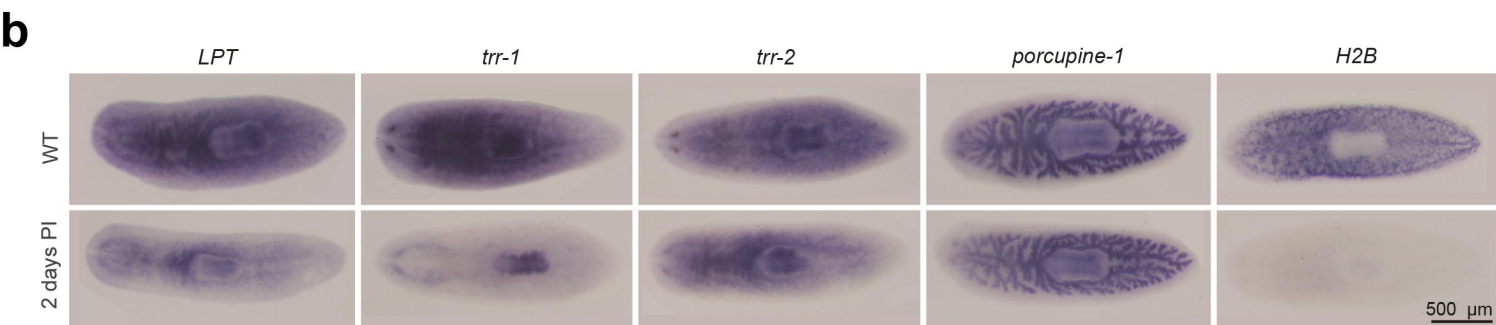
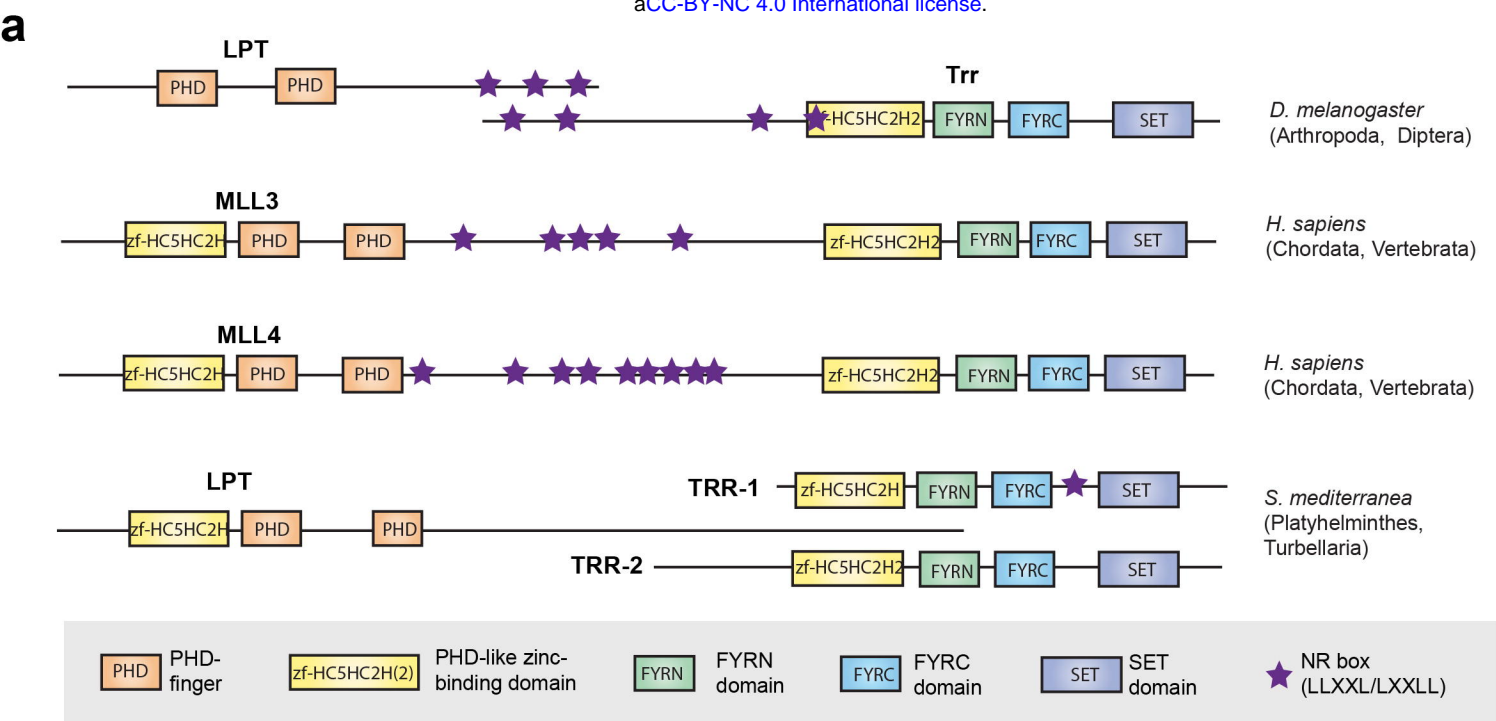
1458 **Additional File 21.** (.xlsx) **Primer sequences.** All primers are given in 5'->3'  
1459 orientation. 'F' and 'R' stand for 'forward' and 'reverse' primer respectively.

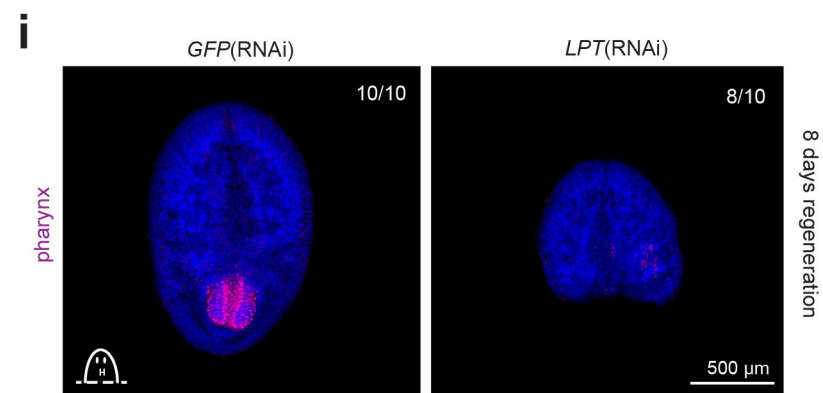
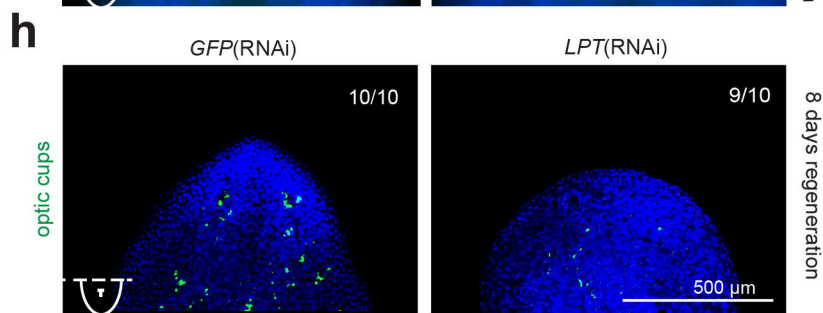
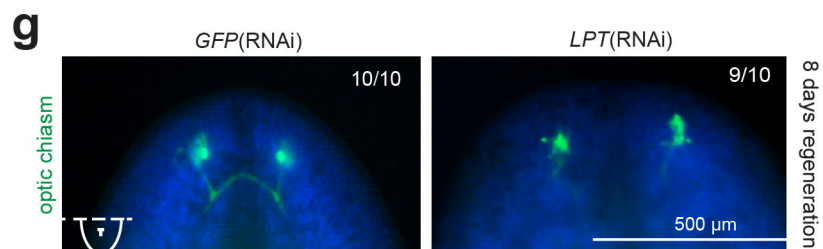
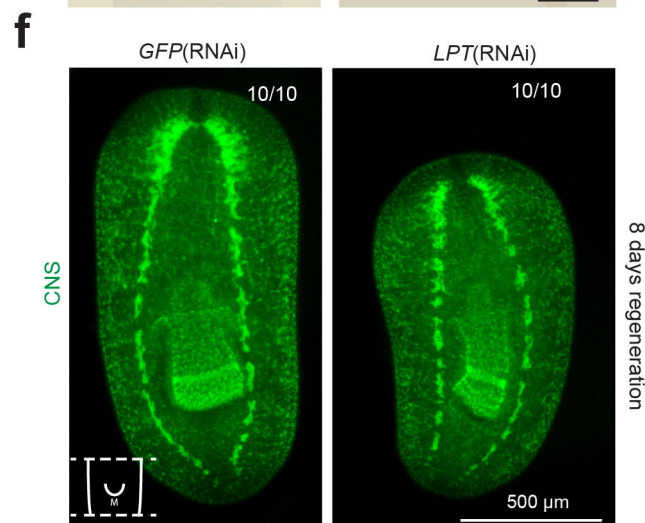
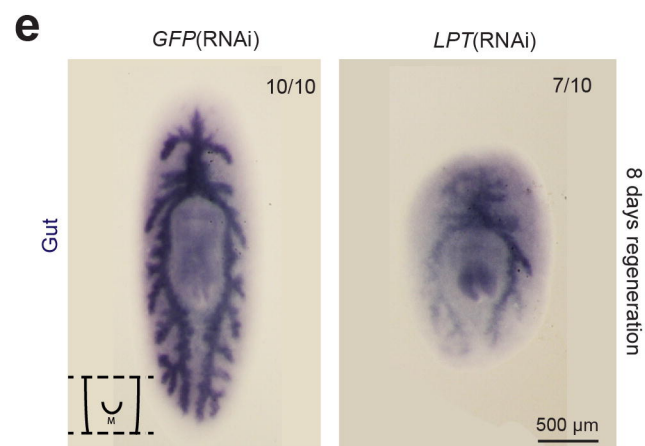
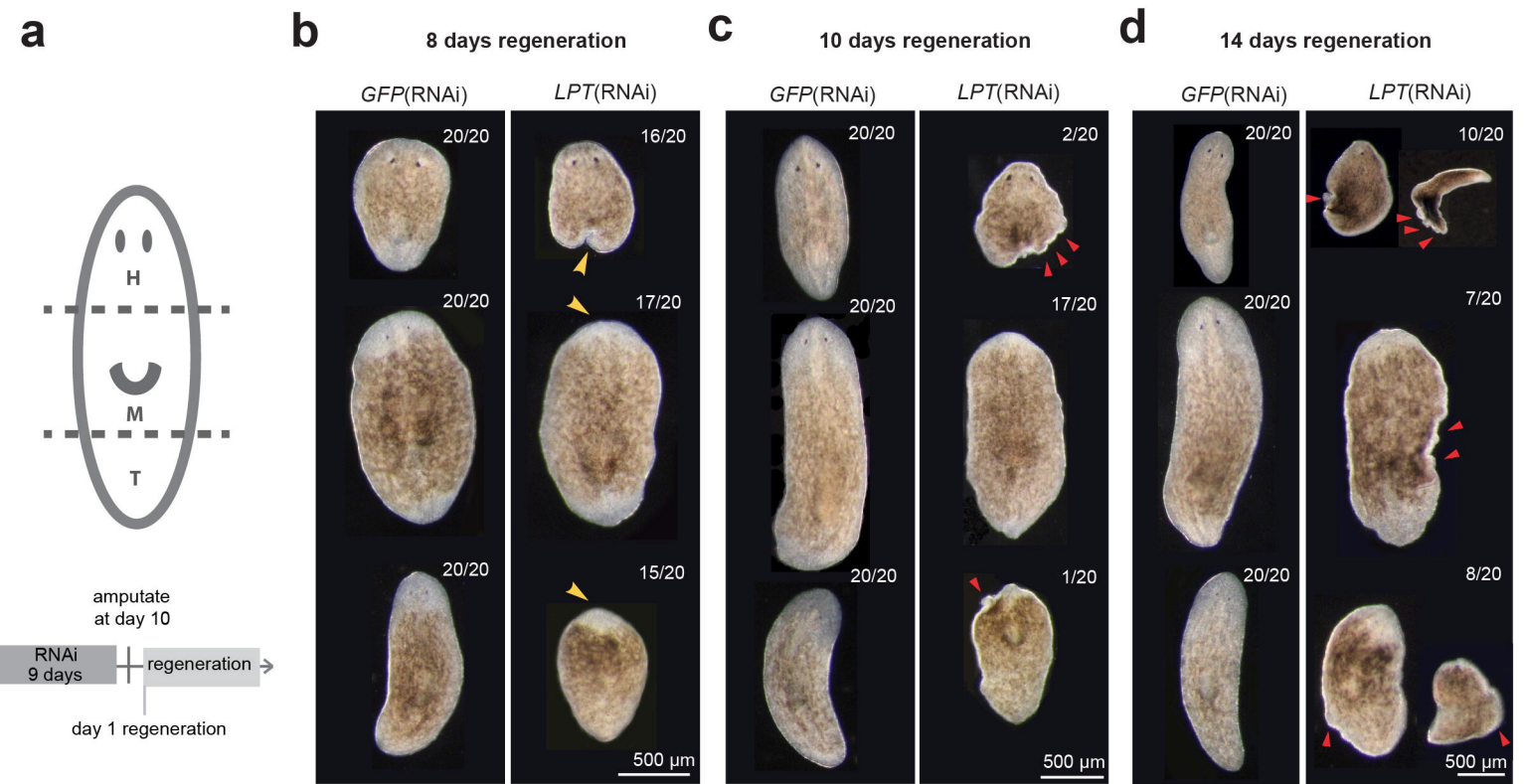
1460

1461 **Additional File 22** (html) Supplementary Python Notebook. Provides details  
1462 on the ChIP-seq and RNA-seq bioinformatic analyses.

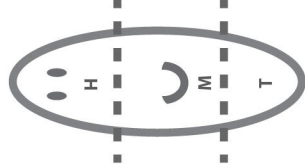
1463

1464

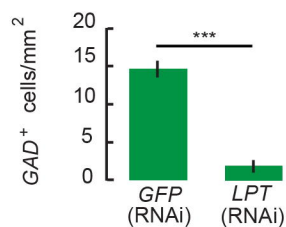
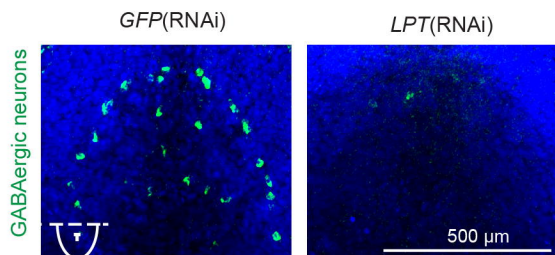




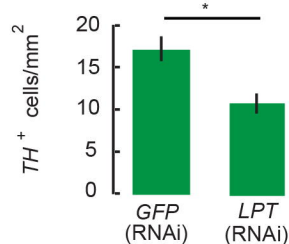
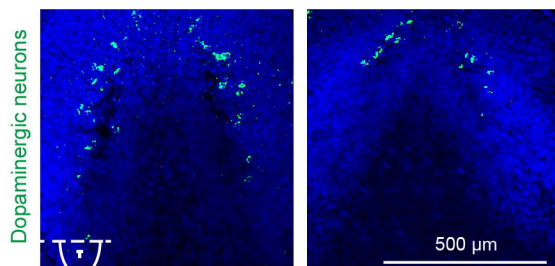
## 8 days regeneration



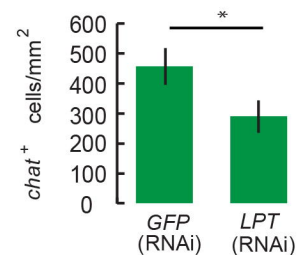
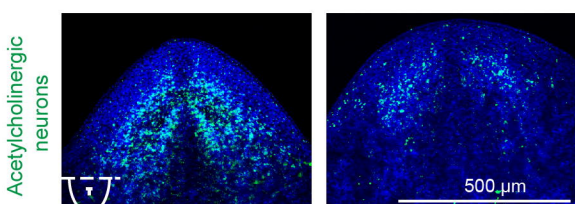
**a**



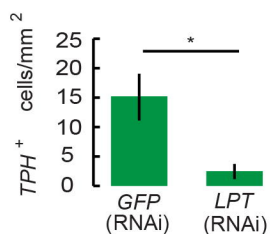
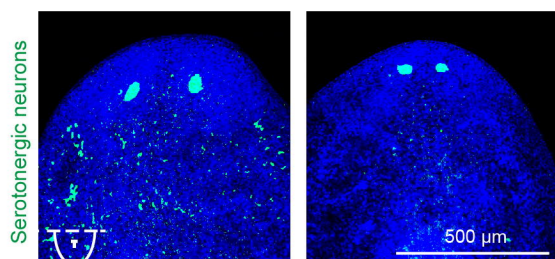
**b**



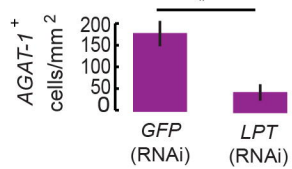
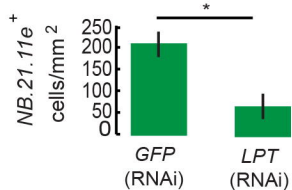
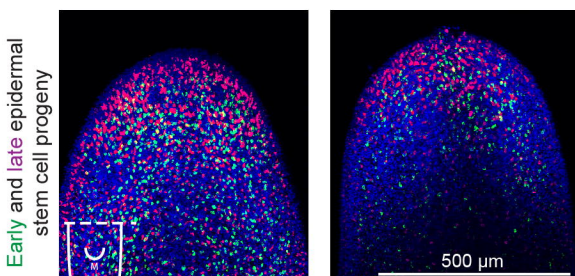
**c**

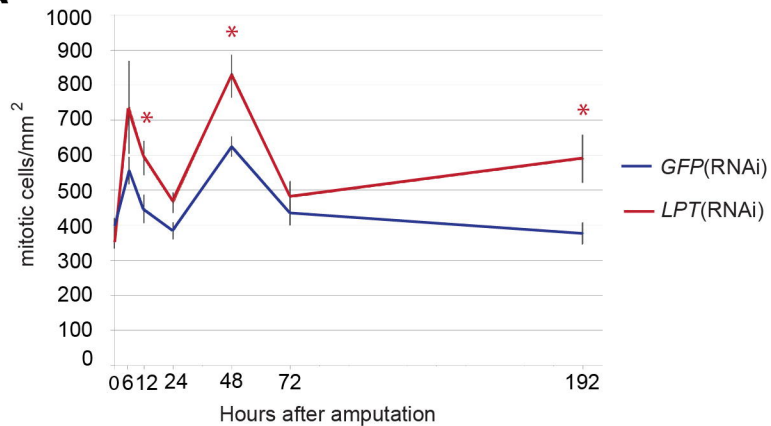
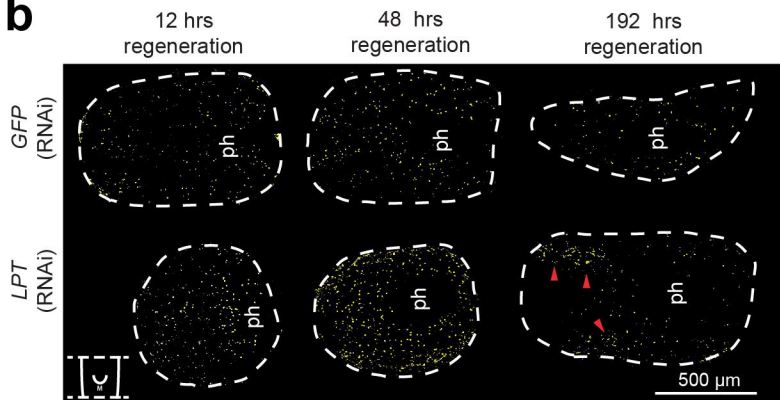
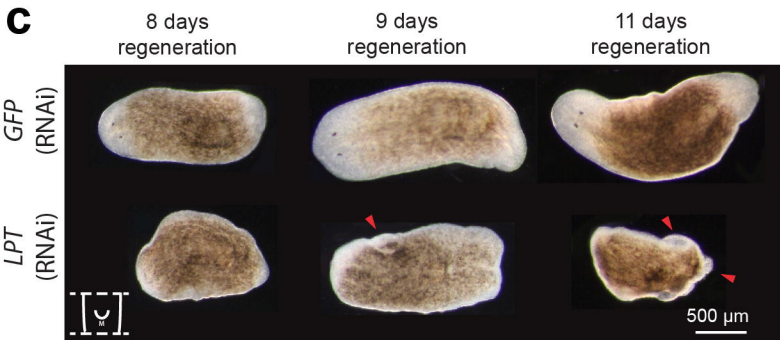
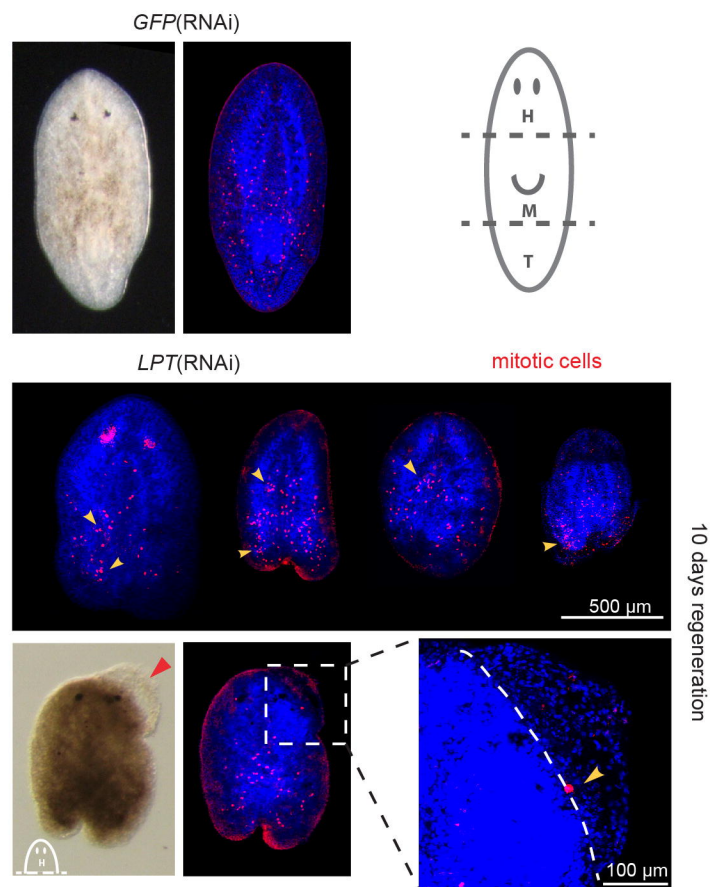
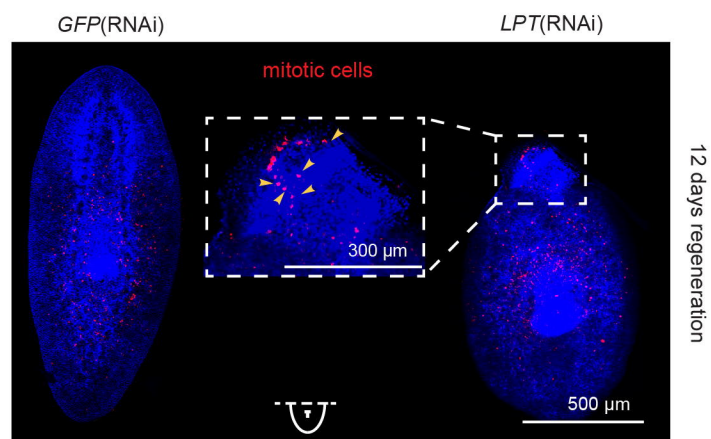


**d**

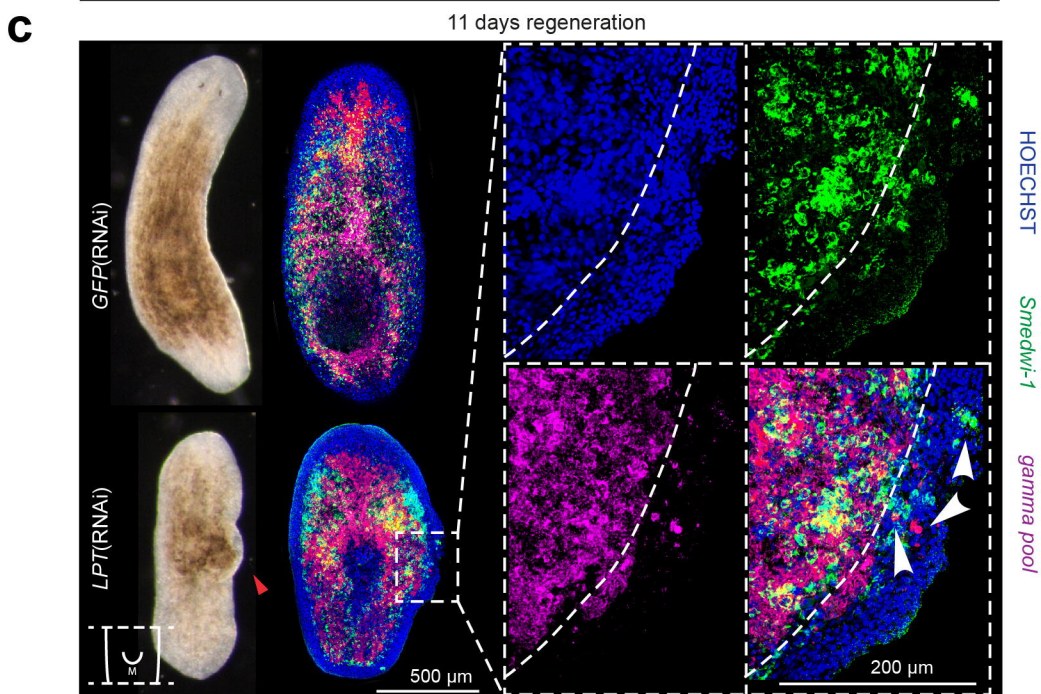
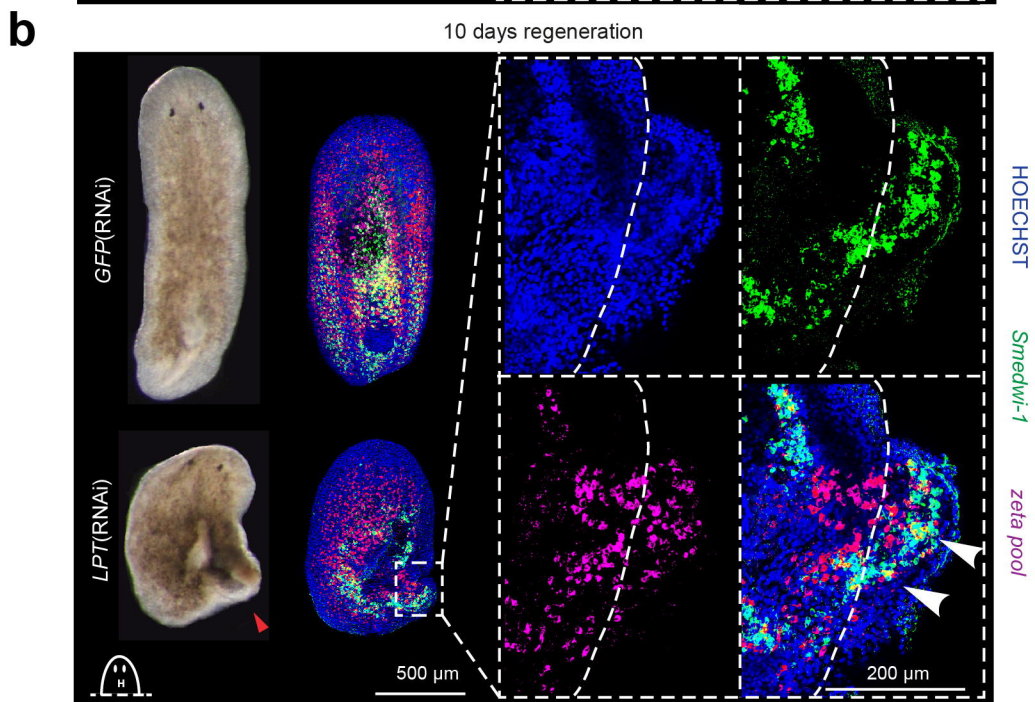
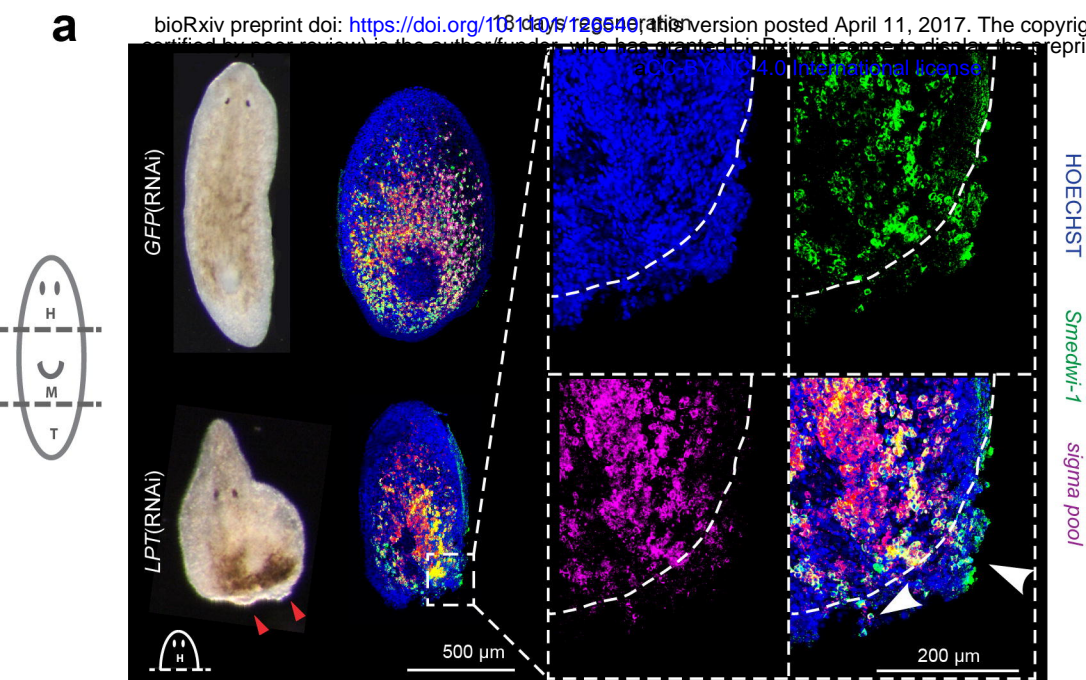


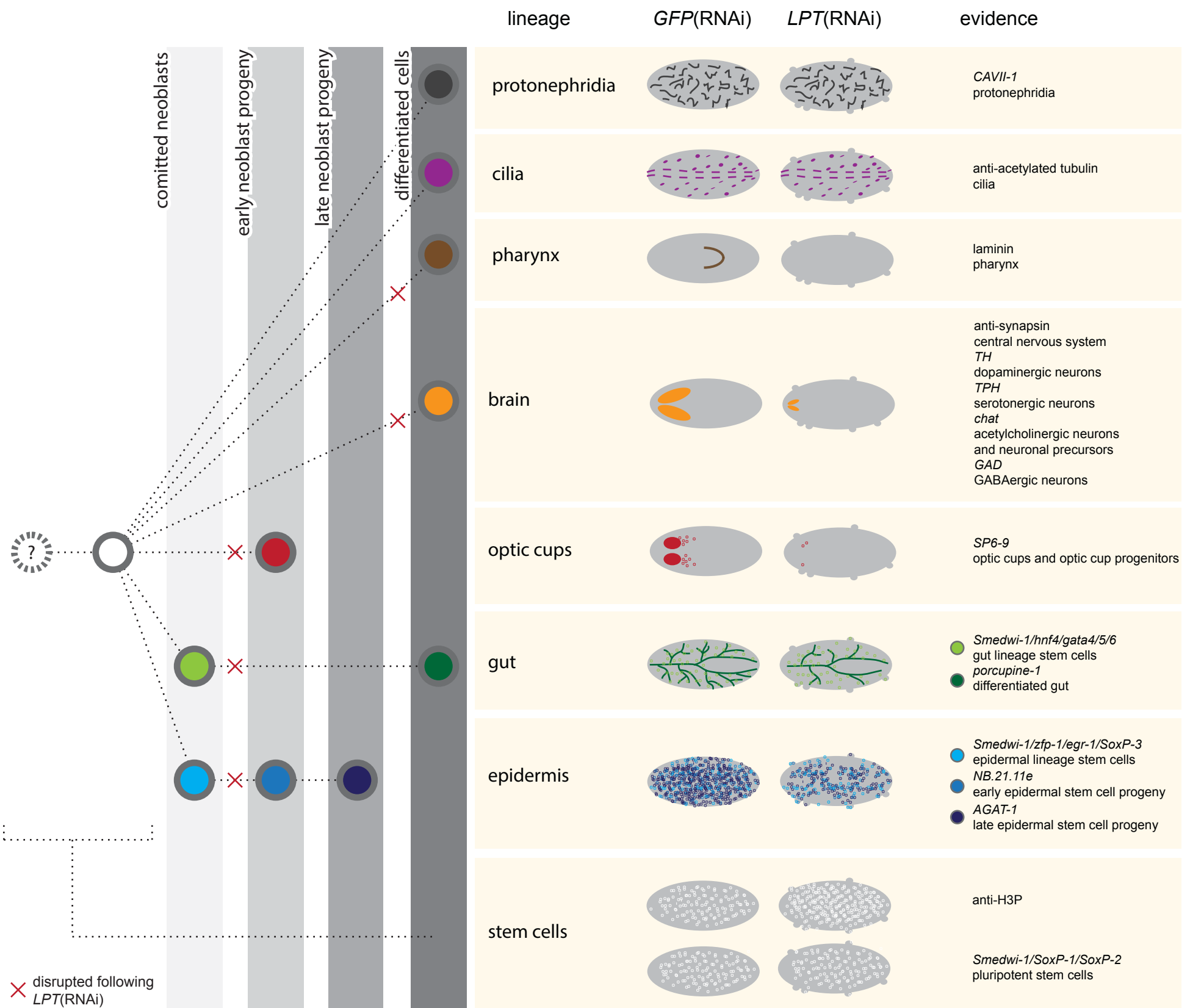
**e**



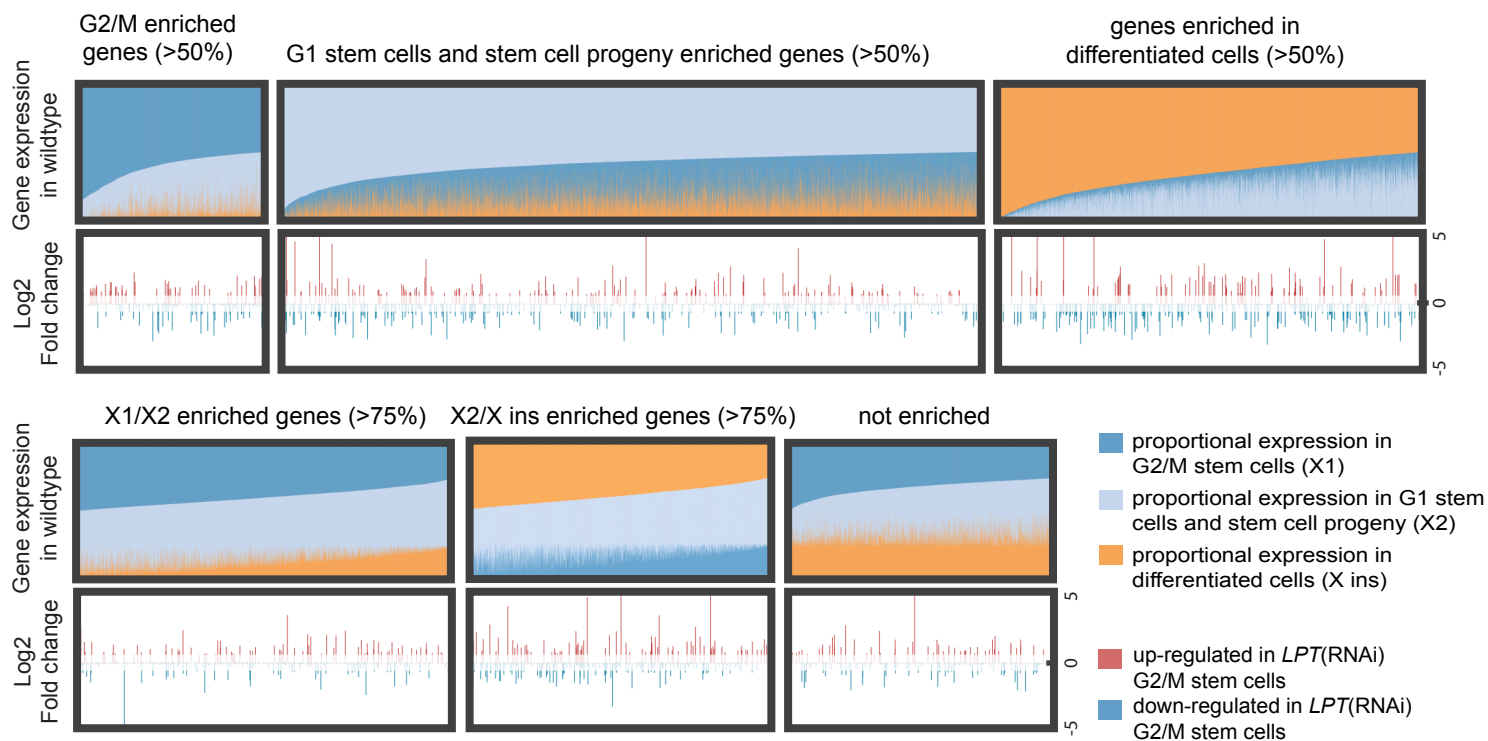
**a****b****c****d****e**







**a**



**b**

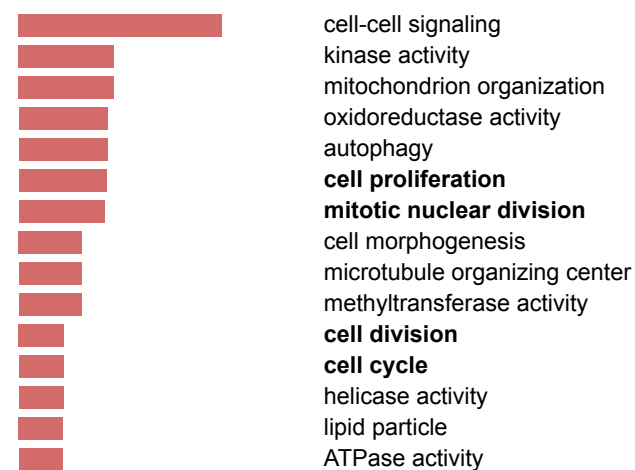
**Number of genes up/down-regulated according to cell population and putative Transcription Factors**

	X1 (2,253)	X2 (8,444)	X ins (5,119)	X1/X2 (4,538)	X2/X ins (3,652)	not enriched (3,200)	TFs (489)
<b>up-regulated (542)</b>	49	160	86	83	79	57	18
<b>down-regulated (540)</b>	37	174	155	44	76	42	29

\*white indicates significant enrichment (p-value < 0.01)

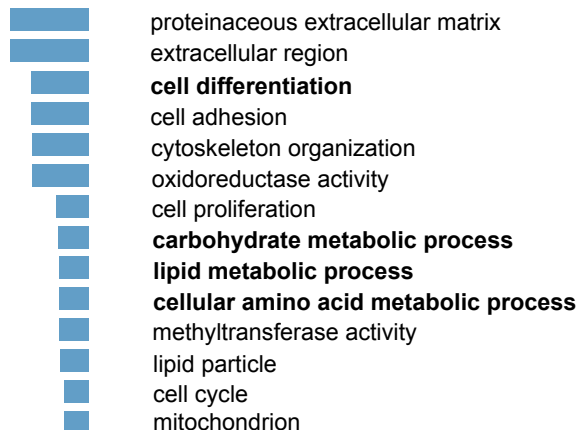
**c**

**GO enrichment RNA-seq up-regulated genes in *LPT*(RNAi) G2/M stem cells**

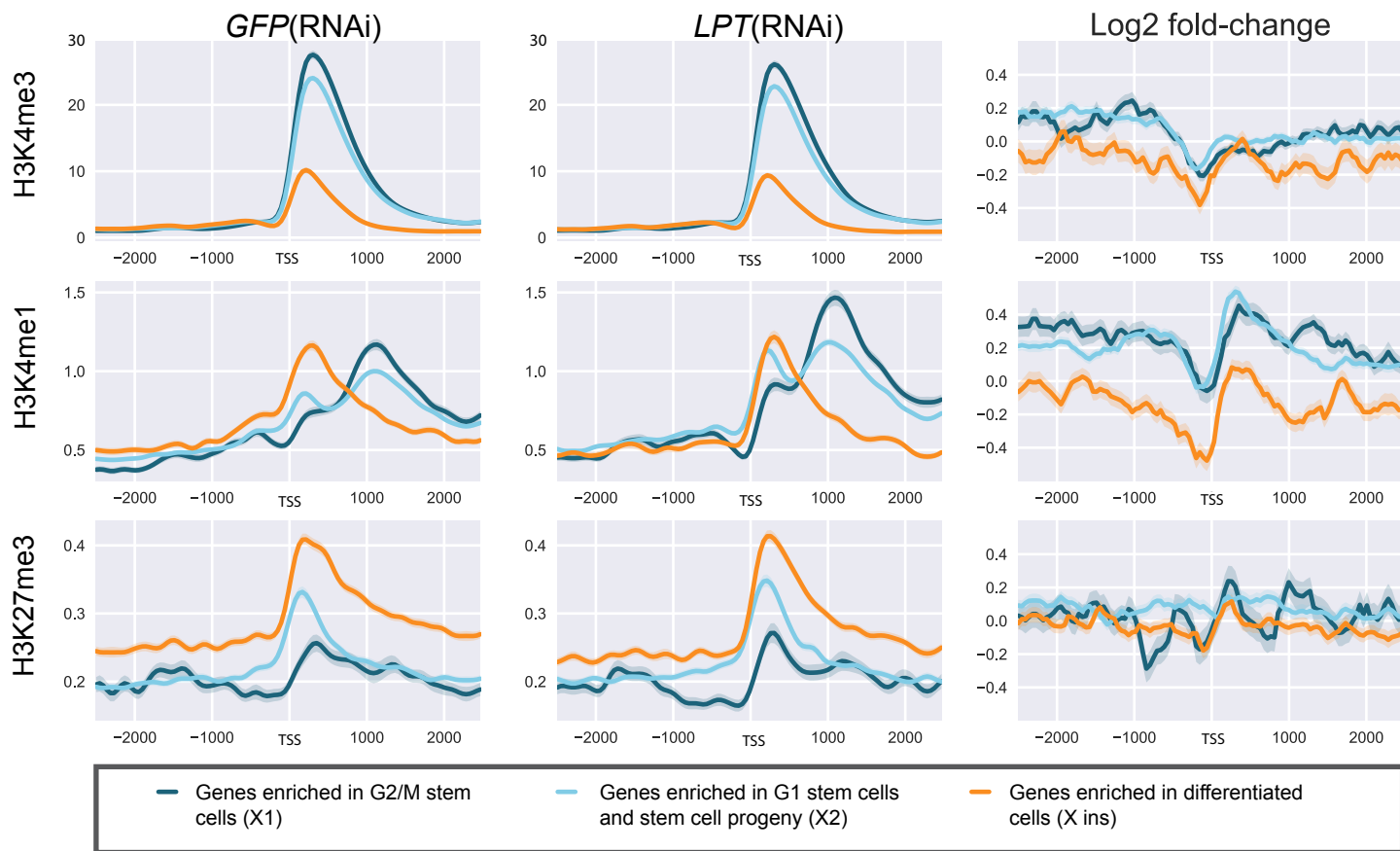
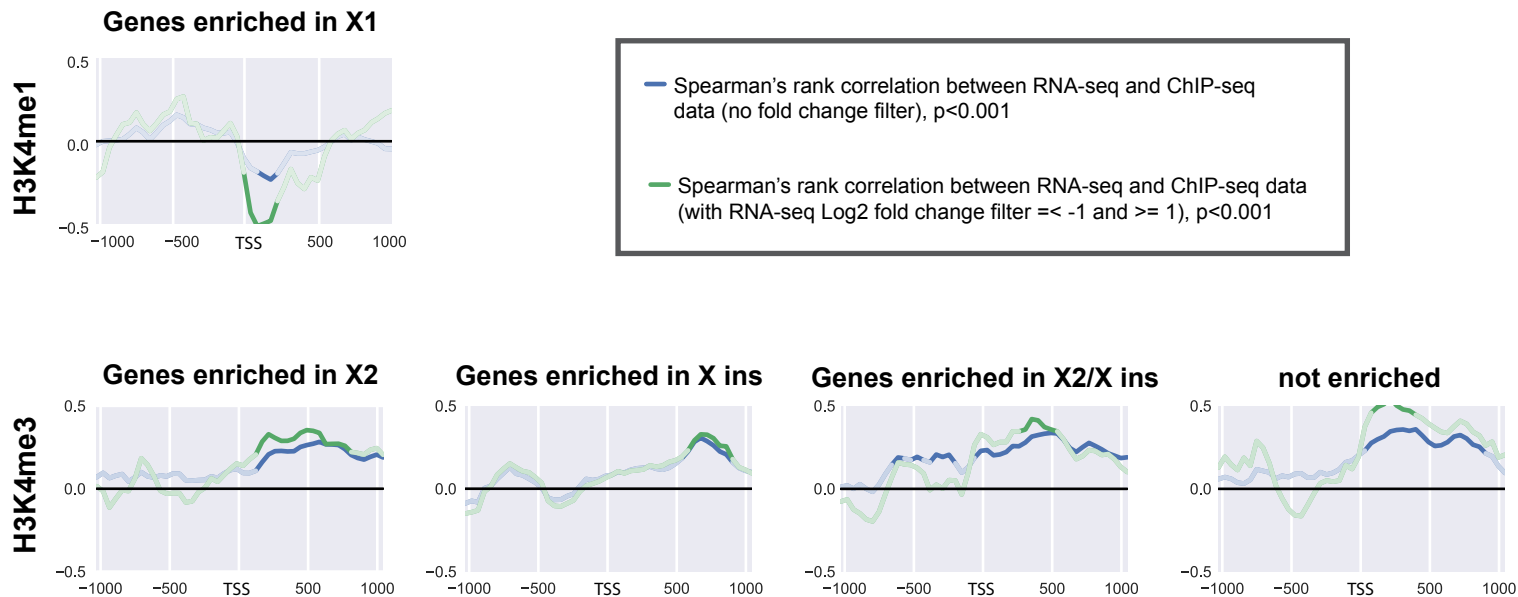


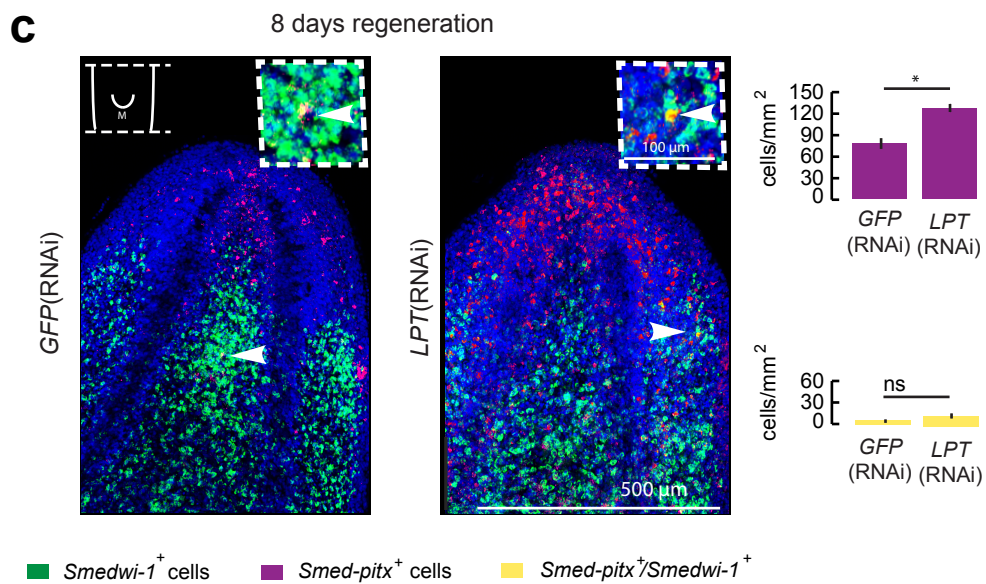
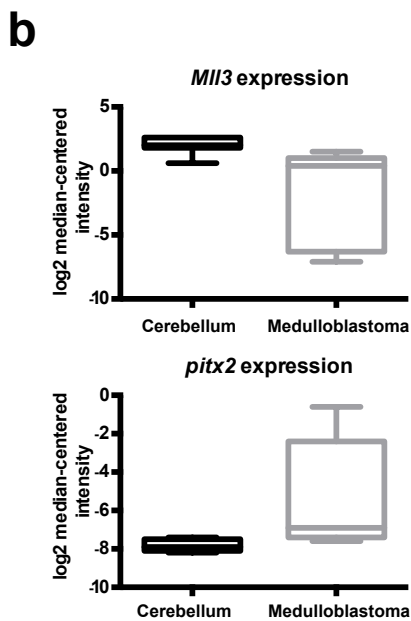
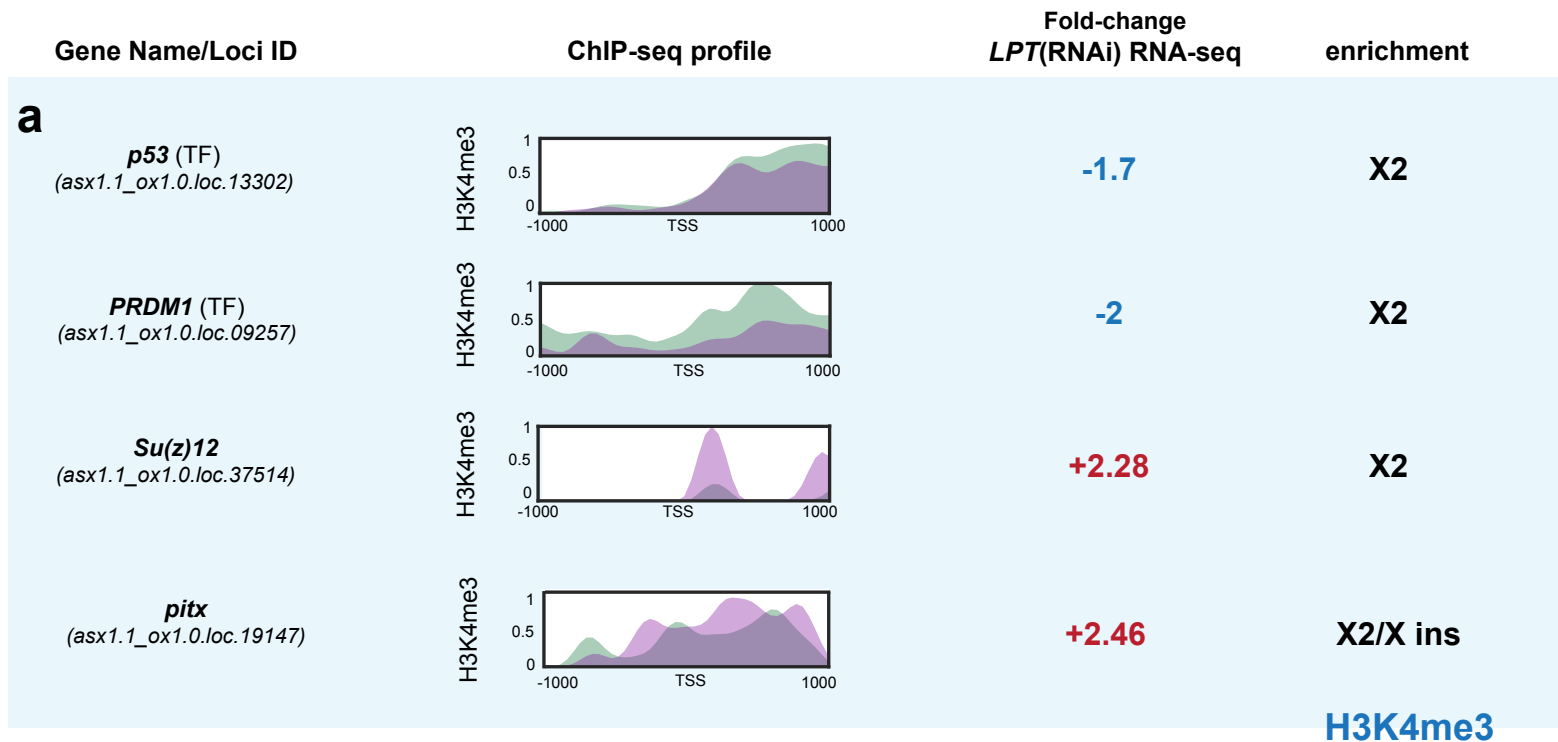
Average Log<sub>2</sub> Fold Change

**GO enrichment RNA-seq down-regulated genes in *LPT*(RNAi) G2/M stem cells**



Average Log<sub>2</sub> Fold Change

**a****b**



normalised ChIP-seq signal following *LPT*(RNAi)

normalised ChIP-seq signal following *GFP*(RNAi)

Gene Name/Loci ID

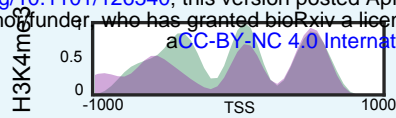
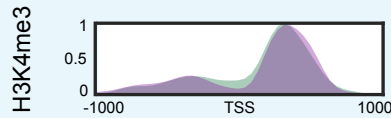
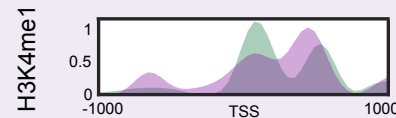
ChIP-seq profile

Fold-change  
*LPT*(RNAi) RNA-seq

enrichment

a

bioRxiv preprint doi: <https://doi.org/10.1101/126540>; this version posted April 11, 2017. The copyright holder for this preprint (which was not certified by peer review) is the author/funder, who has granted bioRxiv a license to display the preprint in perpetuity. It is made available under aCC-BY-NC 4.0 International license.

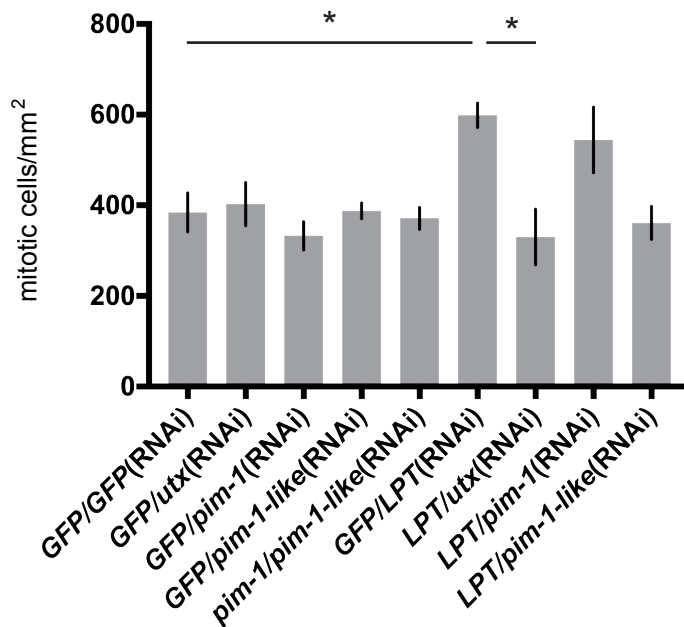
*utx*  
(*asx1.1\_ox1.0.loc.29616*)**+2.2****X2***pim-1*  
(*asx1.1\_ox1.0.loc.12499*)**+2.7****X2/X ins****H3K4me3***pim-1-like*  
(*asx1.1\_ox1.0.loc.18774*)**+3****X1****H3K4me1**

**Bold font** = correlation between  
RNA-seq and ChIP-seq data

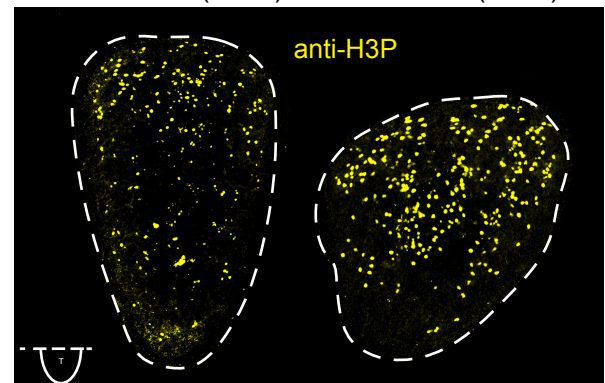
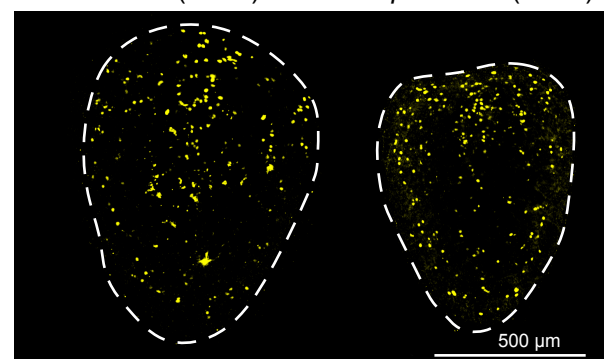
normalised ChIP-seq signal following *LPT*(RNAi)normalised ChIP-seq signal following *GFP*(RNAi)

b

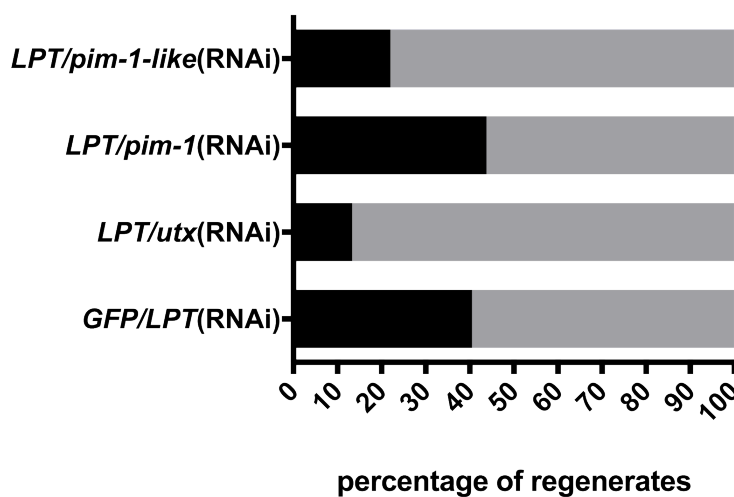
48 hours post-amputation



GFP/GFP(RNAi)

GFP/*LPT*(RNAi)*LPT*/*utx*(RNAi)*LPT*/*pim-1-like*(RNAi)

c



■ No outgrowths  
■ Outgrowths

